

A DEEP IMAGING AND SPECTROSCOPIC SURVEY OF FAINT GALAXIES

S. J. LILLY,¹ L. L. COWIE,¹ AND J. P. GARDNER¹

Institute for Astronomy, University of Hawaii, 2680 Woodlawn Drive, Honolulu, HI 96822

Received 1990 May 9; accepted 1990 August 22

ABSTRACT

The results of a deep imaging and spectroscopic optical survey are presented. Three small areas of sky at 13 h, 17 h, and 22 h have been imaged to faint levels in four passbands (U' , B , V , and I) in the optical window. These reach approximately 27th magnitude for galaxy images, at which point the surface density of galaxies is roughly $2.5 \times 10^5 \text{ deg}^{-2}$. A complete catalog of objects to $I_{AB} \sim 24.5$ is provided as the basis for future studies of the faint extragalactic population. Spectroscopic observations of a small but essentially complete sample of galaxies in and around the 22 h field have yielded redshifts for a high fraction of galaxies with $B_{AB} < 24.1$. Detailed comparison of our deep images with similar data from other observers shows some broad similarities but also some significant differences. In particular, our faintest galaxies are in general considerably redder, and the fraction of galaxies with colors that are unrepresentable by normal galaxies is correspondingly much smaller. We also see evidence for a decline in the steep slope of the B -band number counts for magnitudes fainter than $B \sim 24$. The spectroscopic and imaging data indicate that the median redshift for $B \leq 24$ galaxies is still low, $\langle z \rangle \sim 0.4$, and close to that predicted from nonevolving models of the local galaxy population, despite the substantial enhancement that is seen in the galaxy number counts relative to these same models. A nonparametric analysis confirms that this excess relative to the nonevolution case persists even if the faint galaxy population is used to define the “nonevolving” population, emphasizing that the effect is not caused by a gross misrepresentation of the true local population. The general relationship between the surface number density of a sample of galaxies and their modal redshift is discussed for various parametric forms of the evolution of the luminosity function. The low redshifts encountered at $B \sim 24$ extend the trend noted by other workers to considerably fainter levels, and this indicates that the evolution for galaxies to $z \sim 0.5$ is best characterized as an increase in the apparent ϕ^* rather than in L^* . Some mechanisms for producing an apparent increase in ϕ^* are reviewed, including luminosity-dependent luminosity evolution, an incorrect cosmological volume element, and the possibility of seeing galaxies that have subsequently disappeared in the sense of failing to meet the detection criteria for local galaxies. One of the faint and very blue “flat-spectrum” galaxies in this field has the spectrum of an extragalactic H II region at $z = 0.13$, but the other two remain stubbornly unidentifiable, including SSA 22-24, for which we had earlier suggested a redshift of 3.3 which we are not able to confirm. The nature of these flat-spectrum objects is discussed, and it is concluded that a high-redshift population remains the most likely, but unproved, explanation. Finally, we explore the implications of the very high number surface density of galaxies seen at 26th magnitude and highlight the difficulties of accounting for these galaxies with models that conserve the numbers of galaxies.

Subject headings: galaxies: evolution — galaxies: formation — galaxies: photometry — galaxies: redshifts

1. INTRODUCTION

The advent of optical CCDs and of infrared array detectors has opened a new era in the study of faint galaxies. The use of self-calibration techniques to flatten the images from these devices has meant that the achievable depth is limited only by the amount of time available on large telescopes. Furthermore, the recent availability of two-dimensional infrared images now enables the whole of the ground-based atmospheric window from 3200 Å to the onset of the thermal infrared at 2.2 μm to be covered.

A number of groups are pursuing survey projects with the aim of understanding the properties of the faintest galaxies detectable. It is anticipated that important insights into the galaxy formation process and the way in which galaxies have subsequently evolved to their present appearance will be gained through these studies.

In this paper, we present and discuss the optical part of a deep survey carried out under the superb observing conditions of Mauna Kea. The optical part of the survey was carried out on the 3.6 m Canada-France-Hawaii Telescope (CFHT) and the 2.2 m University of Hawaii Telescope. Deep images in U' , B , V , and I have been obtained which reach limiting 1σ photometric AB magnitudes for galaxies (i.e., in 3"0 apertures) of about 27th magnitude. In addition, infrared images are being obtained with the 3.8 m United Kingdom Infrared Telescope which reach a limiting AB magnitude that is only 2 mag brighter than the optical limit (i.e., $K_{AB} \sim 25$) and which detect a comparable surface density of galaxies. A full discussion of the infrared data is presented elsewhere (Cowie et al. 1990).

Three small areas of the sky, each approximately 70" square, have currently been surveyed to these deep optical levels. Each is surrounded by an area roughly 5' square which is also being studied to a shallower depth in both the optical and infrared. This shallow survey is still underway and will be reported elsewhere (Gardner et al. 1991). In addition to the deep images, optical spectroscopy of selected galaxies has been started with the CFHT with the initial goal of securing redshifts for a com-

¹ Visiting Astronomer at the Canada-France-Hawaii Telescope, which is operated by the National Research Council of Canada, the Centre National de la Recherche Scientifique of France, and the University of Hawaii.

plete sample of $B \leq 24$ mag galaxies. Initial results from this spectroscopic program are discussed in detail in this paper.

These deep fields form an ideal basis for the study of faint field galaxies at other wavelengths. The *Hubble Space Telescope* will be used to extend the wavelength coverage of the survey down to 2500 Å, and high-resolution optical images may also eventually be obtained. These fields will also form the basis for future studies at other wavelengths. Consequently, a comprehensive and statistically complete photometric catalog of objects down to a limiting magnitude of $I_{AB} < 24.5$ is given in this paper.

The paper is arranged as follows. In § 2 we discuss the selection of the survey fields and the basic observational material and present the complete $I_{AB} < 24.5$ catalog. In § 3 we discuss basic features of the data, such as the number-magnitude counts, the color-magnitude diagrams, and the image profiles of typical faint galaxies, with particular reference to the generally comparable data of Tyson (1988). In § 4 we discuss the survey results in the context of current ideas and questions concerning galaxy formation and evolution. Finally, we summarize the paper in § 5. A Hubble constant of $50 \text{ km s}^{-1} \text{ Mpc}^{-1}$ is taken throughout the paper.

2. OBSERVATIONS

2.1. Survey Field Selection

The field size for each Small Selected Area (SSA) was chosen to be around 1 arcmin^2 , so that they could be covered by a 60×60 pixel infrared array at about $1'' \text{ pixel}^{-1}$. This field size was also well matched to the size of our 800×800 TI CCD operating in an unreduced mode at the $f/10$ focus of the 3.6 m Canada-France-Hawaii Telescope and at the $f/8$ focus of the 2.2 m University of Hawaii Telescope. The resulting pixel scales of $0''.11 \text{ pixel}^{-1}$ and $0''.13 \text{ pixel}^{-1}$, respectively, allow full oversampling of the best images expected from Mauna Kea. The absence of intervening optics also maximizes throughput and maintains the highest possible image quality. The oversampling not only preserves image quality but also offers considerable advantages in the removal of many of the CCD defects which generally have scale sizes of only a pixel or two. Each SSA was defined to be a square region of sky $70''0$ on each side.

A number of these SSAs were set up around the sky. To ensure randomness, these were selected to lie at the interstices of the coordinate grid on the Ohio overlays of the National Geographic Palomar Sky Survey. At approximately each hour of right ascension, one such intersection was chosen that was apparently free of objects on the print copies in a $3' \times 3'$ region of sky. Zwicky clusters were avoided and no fields at Galactic latitude $b < 30^\circ$ were selected. The fields in the range $21^{\text{h}} < \text{R.A.} < 05^{\text{h}}$ were chosen to be close to the equator, and those in the range $09^{\text{h}} < \text{R.A.} < 17^{\text{h}}$ at $\delta \sim 40^\circ$, in order to reach high Galactic latitude. In this paper, we report deep imaging observations of three of these SSAs, those at 13^{h} , 17^{h} , and 22^{h} , which we henceforth refer to as SSA 13, SSA 17, and SSA 22. The coordinates of these fields may be found in Table 1. We also have initial spectroscopic observations of a small but essentially complete subsample of faint galaxies in and around the SSA 22 field.

2.2. Deep Optical Imaging Observations

Deep optical images of these three fields have been obtained using the 3.6 m CFHT and the UH 2.2 m telescope on Mauna

TABLE 1
SMALL SELECTED AREA SURVEY FIELDS

Field	R.A. (1950)	Decl.(1950)	b	l
SSA 13.....	$13^{\text{h}}10^{\text{m}}01^{\text{s}}.24$	$+43^{\circ}00'32''.6$	73	109
SSA 17.....	17 04 59.81	$+43 59 34.7$	36	68
SSA 22.....	22 15 01.00	$+00 00 05.8$	-45	65

Kea. In each field we now have images in four optical bands, U' , B , V , and I . This data set has been built up during a number of observing runs between 1987 July and 1989 July. Further optical imaging data on these fields are being acquired to continue to deepen the images. Most of the imaging was carried on the CFHT, with the UH 2.2 m employed to fill in the gaps and nonuniformities in our coverage.

For all observations, the University of Hawaii NSF1 TI 800×800 CCD camera was used at direct Cassegrain focus, giving a pixel scale of $0''.11 \text{ pixel}^{-1}$ on CFHT and $0''.13 \text{ pixel}^{-1}$ on the UH 2.2 m. In order to employ statistical sky-flattening techniques, each observation was split into a number of shorter exposures, between which the telescope was offset by a small amount so that the center of the images moved around a small pattern on the sky. Each of these images was timed so that the dominant source of noise would be the photon noise of the sky background. Because of the small field of view of our configuration ($90'' \times 90''$ on the CFHT) the positional offsets were limited to be $\pm 20''$ from the center, and the typical spacing between points in the mosaic was about $10''$. The sky-flattening techniques used on these data will therefore destroy information on structure in the sky on scales of $10''$ and larger.

All of the subsequent reduction and analysis steps were undertaken by two of the authors independently, using different software packages on different computer systems. After initial flattening with dome flats, two low-level cosmetic defects were removed prior to the generation of sky flats. These were (1) an effective nonlinearity that affected all pixels in a column equally and (2) a charge transfer problem in a swath of columns that resulted in the pixels of a given row within this area having a small offset relative to other rows. Both of these were small effects (about 1% of sky) and were satisfactorily removed by applying a small multiplicative correction to the affected rows and columns. This was done prior to the production of sky flats because the amplitude of the first effect depended on the sky level and because the pattern of the second was nonrepeatable.

Subsequently, sky flats were generated from the images by first normalizing them to a standard sky level and then determining the median value of each pixel. A minimum of nine images were used in this process, and usually many more. In the case of the I images, up to 50 exposures of 5 minutes were included in this process. In order to reach the sky background in a sufficiently short time to obtain enough individual images for the median sky-flat process, the U' and B images were taken in a 2×2 binned mode. After division of all images by the sky flat and subtraction of a uniform sky background level from each image, all images were co-registered to the nearest pixel and then averaged. The averaging algorithm included a filter to exclude pixels with anomalously high values, since these were likely to be cosmic-ray events. Finally, to prepare the images for photometric analysis, a precise residual sky background frame was generated by smoothing the final image

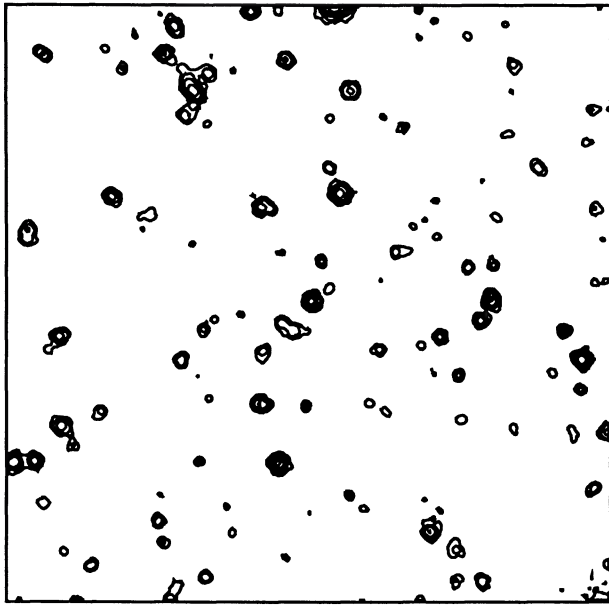


FIG. 1b

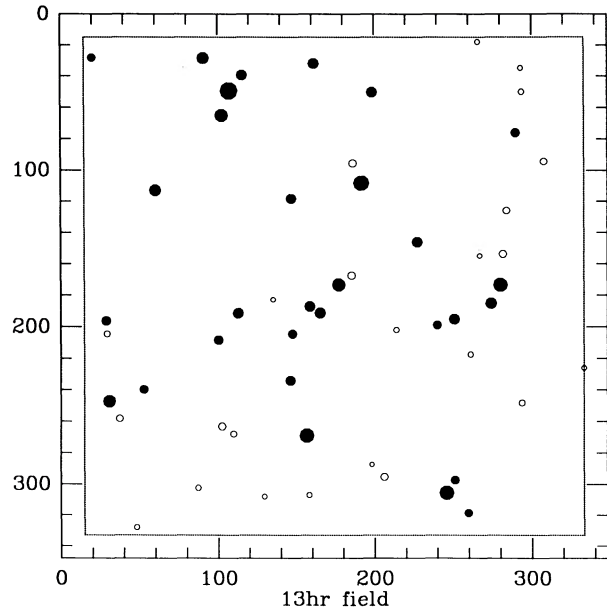


FIG. 1c

with a median filter of size approximately $25'' \times 25''$. As expected, this background frame had an average of zero and rarely had a differential amplitude across the image much in excess of 1 electron, equivalent to about 2×10^{-3} of the sky background. This residual sky background frame was subtracted from the final image, which was then rotated, stretched, and clipped as required to be co-registered with all of the other images of that SSA. In all procedures except the last residual sky determination, multiplicative corrections were applied. No evidence for night-sky fringing, which might have warranted an additive correction, was seen. In any case, for all steps except the initial dome flattening, the correction applied to the

data was so small ($\sim 1\%$) that the difference between an additive and a multiplicative correction is negligible.

Gray-scale plots of the sum of the final U' , B , V , and I images for each of the three fields are shown in Figures 1a, 2a, and 3a (Plates 2-4). Contour representations of these summed images are shown in Figures 1b, 2b, and 3b.

Photometric calibration was made with observations of the fainter Landolt (1983) equatorial standards for B , V , and I , and of spectrophotometric standards from the lists of Oke (1972) and Stone (1977) for U' . The effective wavelength of the U' filter was shown to be 3400 \AA , as expected, and its calibration was put straight onto the AB system [$AB = 48.60 - 2.5 \log f_\nu$ (cgs

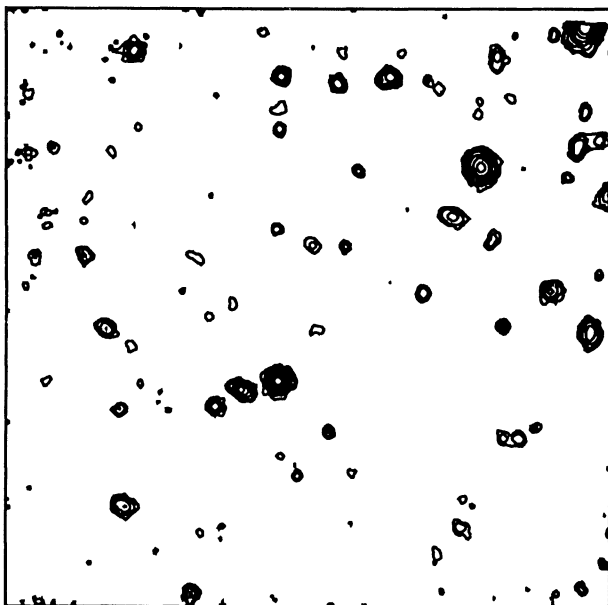


FIG. 2b

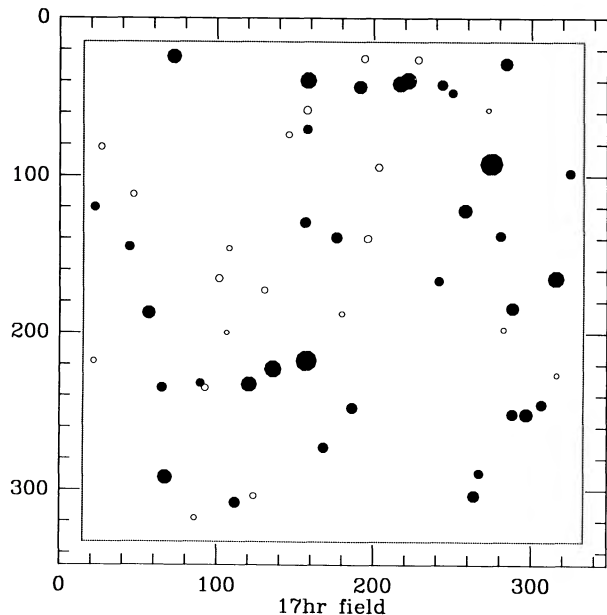


FIG. 2c

PLATE 2

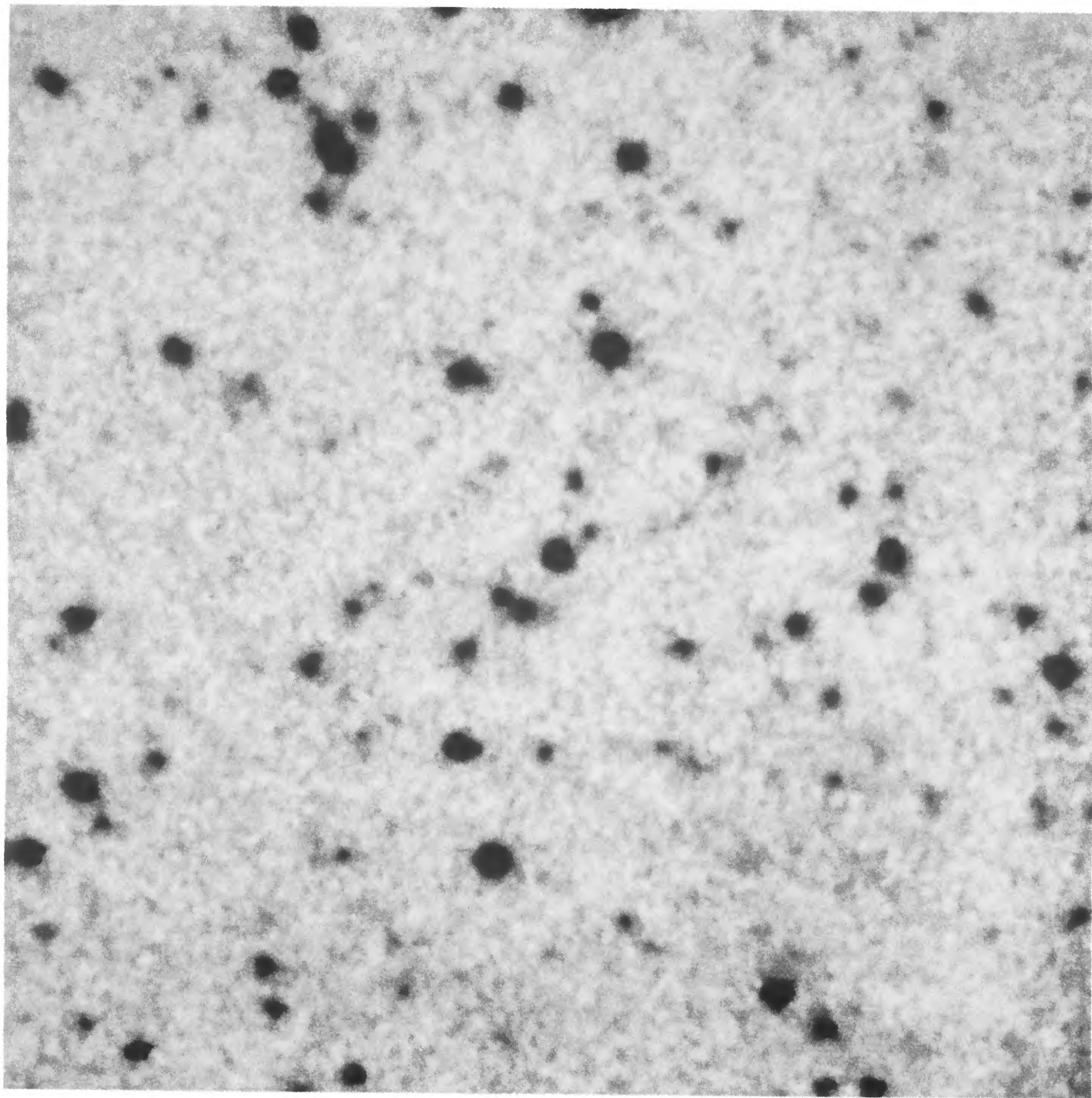


FIG. 1a

FIG. 1.—(a) Gray-scale image of summed U , B , V , and I images of SSA 13 (b) Contour plot of summed U , B , V , and I images of SSA 13. (c) Identifications of cataloged images in SSA 13.

LILLY, COWIE, & GARDNER (see 369, 81)

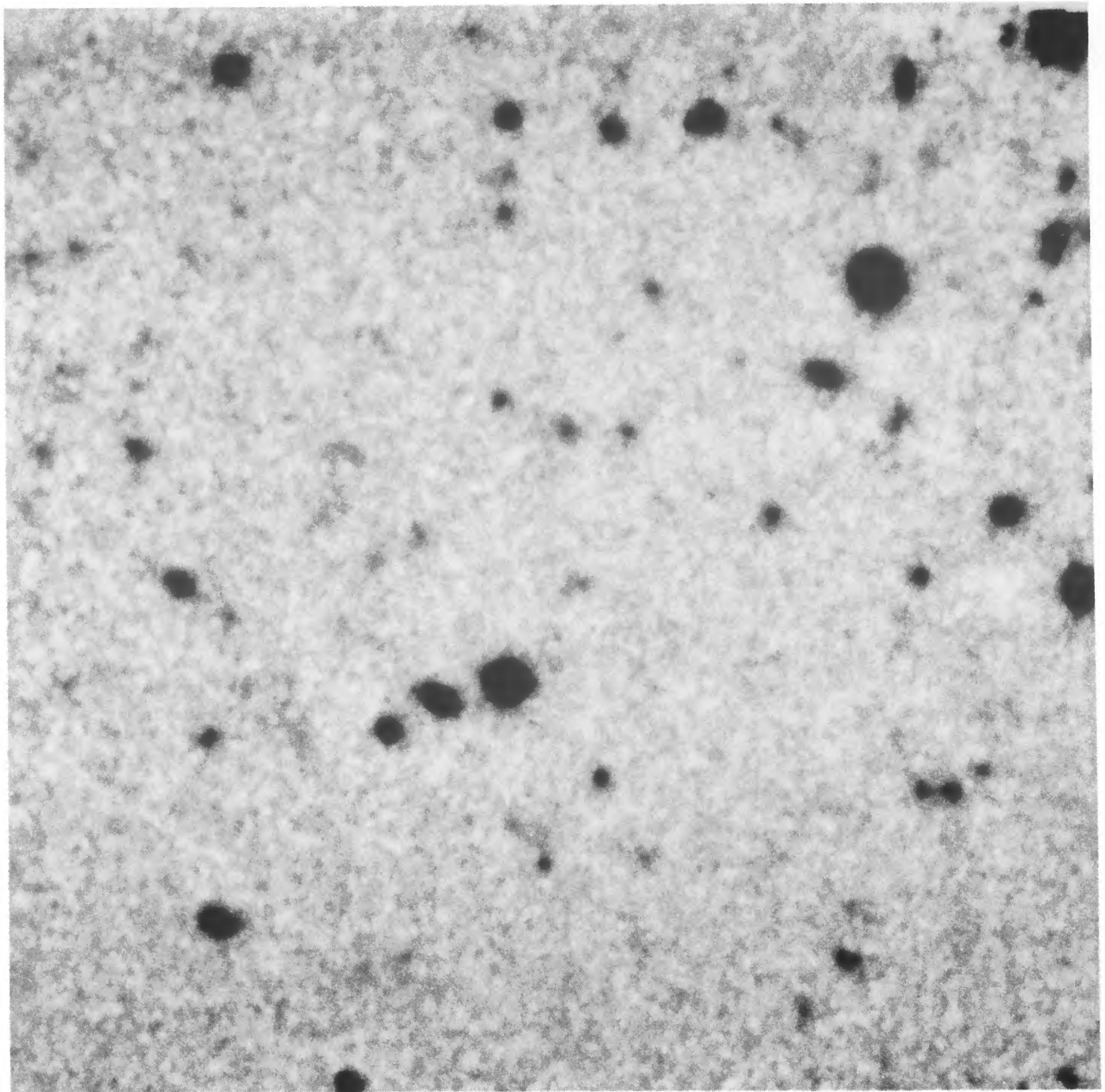


FIG. 2a

FIG. 2.—(a) Gray-scale image of summed U' , B , V , and I images of SSA 17 (b) Contour plot of summed U' , B , V , and I images of SSA 17. (c) Identifications of cataloged images in SSA 17.

LILLY, COWIE, & GARDNER (see 369, 81)

PLATE 4

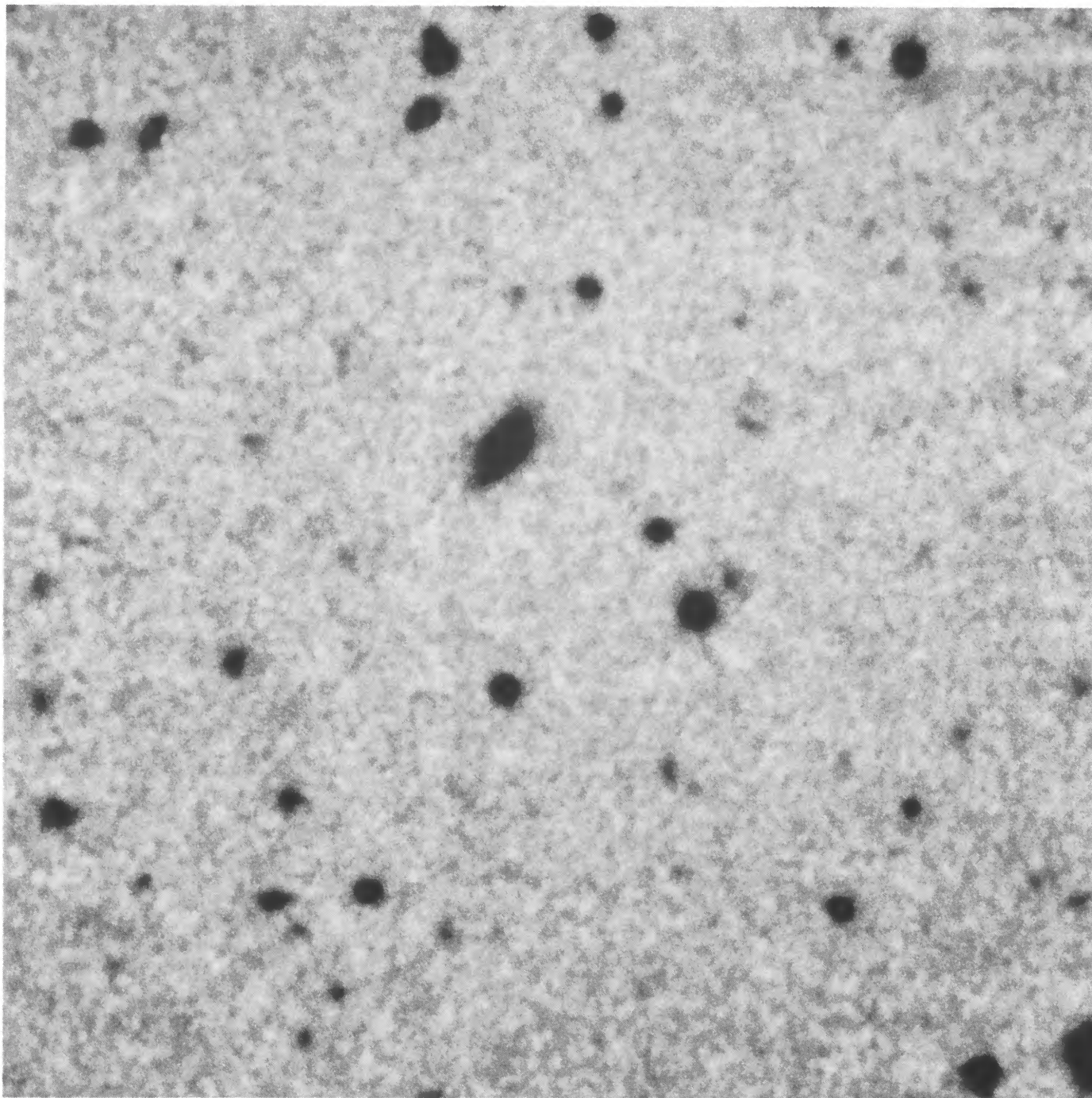


FIG. 3a

FIG. 3.—(a) Gray-scale image of summed U' , B , V , and I images of SSA 22 (b) Contour plot of summed U' , B , V , and I images of SSA 22. (c) Identifications of cataloged images in SSA 22.

LILLY, COWIE, & GARDNER (see 369, 81)

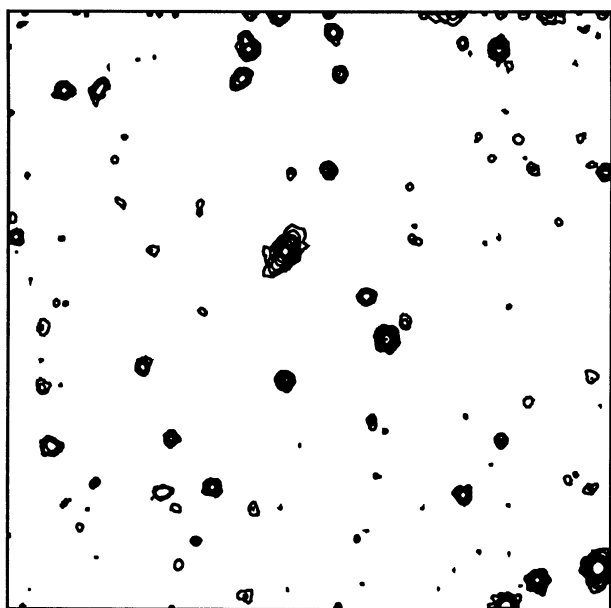


FIG. 3b

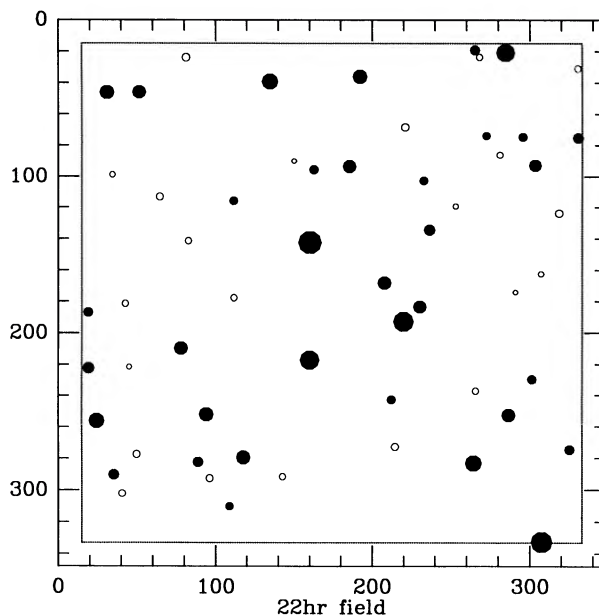


FIG. 3c

units)]. For the other filters, the color equation generated from the Landolt standards was used to determine the effective wavelength of each filter, and the calibration to convert the observed instrumental magnitude to the AB magnitude system at that effective wavelength was computed. In other words, it was decided not to correct the photometric measurements of each object onto one of the standard systems, since the correction for the faintest objects would be necessarily uncertain because their observed colors would be poorly determined, but rather to remain at the observed effective wavelength and to use AB magnitudes whose normalization is independent of wavelength.

The effective wavelengths of these passbands were generally not too far from the standard values and in the range 4600–4700 Å for B , 5500–5600 Å for V , and 8600–8900 Å for I . For reference, the following rough transformations may be used to convert our AB magnitudes onto the α Lyrae system: $B \sim B_{AB} + 0.17$, $V = V_{AB}$, and $I \sim I_{AB} - 0.48$. In practice, our B_{AB} is quite close to a B_j measurement, albeit through a considerably narrower bandpass. The U' filter was designed to be as close as possible to the atmospheric limit while maintaining an accurate calibration. The final design used a 3400 ± 175 Å bandpass tightly blocked at all longer wavelengths. The difference in effective wavelengths and the different widths of the bandpasses between this filter and the standard U is sufficiently large that conversion between the two is not very meaningful.

2.3. Choice of Photometric Approach

The method of photometry adopted in the analysis of faint galaxy images is of considerable importance and merits close attention. Several techniques are applicable and have been used by other investigators. Before describing the construction of the sample of detected objects, we discuss these approaches to faint galaxy photometry.

First, there is straightforward aperture photometry, in which a fixed circular aperture is applied to all objects in all passbands. This has the merit of simplicity, since only the center of

each image needs to be specified, and also of ready “visualization” and repeatability, in the sense that the aperture is always the same for all objects. Provided that the seeing is the same on the different wave-band images, it produces accurate colors in a very straightforward way. Potential drawbacks include the contaminating effects of close neighbors and the different fraction of light included within the aperture for objects of different profiles. The physical size corresponding to the aperture is also a function of redshift, although this will not be a strong effect for $z > 0.5$.

A frequently used alternative is isophotal magnitudes, in which the light is integrated out to some fixed limiting magnitude. This clearly overcomes some of the effects of different image profiles. Nevertheless, there will be a strong redshift dependence on the physical size corresponding to a fixed isophote for a given object because of the $(1+z)^4$ cosmological dimming and K -correction effects, and for fainter objects the fraction of light enclosed within the isophote may drop quite suddenly, especially if the isophotal limit becomes comparable to or smaller than the seeing disk. Contaminating neighbors may still distort the determination of the isophotal profile. The construction of meaningful colors is also difficult, requiring the application of an isophotal aperture determined in one passband to all images. The alternative use of isophotal magnitudes in all passbands (see, e.g., Tyson 1988) requires the application of potentially large and certainly poorly understood corrections to the derived colors. Finally, since the isophote is determined for each object separately, interpretation of the meaning of the quoted magnitudes can be difficult.

Finally, a derivative of the isophotal approach is the use of apertures that are determined from the shape of the light profile (e.g., Kron 1980). If the profile is independent of wave band, then the fraction of light that is enclosed within some characteristic radius should be independent of redshift, although this advantage may be mitigated to a certain degree as objects merge into the seeing disk. The remarks about the determination of colors with isophotal magnitudes apply equally here also. A drawback of this approach is the need to

use the moments of the profile to determine the aperture, which may introduce considerable dispersion in the case of very faint objects.

In the present study, one of the main aims was the study of the population of faint 24th magnitude galaxies through the construction of accurate ($\sigma \sim 0.1$ mag) broad-band colors over a large range in wavelength. Consequently, aperture magnitudes have been determined through a 3" diameter circular aperture for all objects. Prior to this, a Gaussian smoothing was applied to the individual images of each field to bring them to the effective FWHM seeing of the worst image, which was generally 1".2 or better. Thus the aperture diameter of 3" is at least 2.5 times this worst-seeing FWHM.

This aperture encloses a substantial fraction of the light—95% for stellar objects and about 80% even for the largest galaxies—so that the magnitudes of all objects can be inter-compared. It should be noted that use of a relatively large aperture size does not greatly degrade the signal-to-noise ratio (S/N) even when compared with an extraction with optimized S/N. In order to facilitate comparison with the work of others, and recognizing that this fixed aperture systematically underestimates the brightness of the brightest and most extended objects, isophotal magnitudes in the *I* and *B* bands were also measured to the $\mu(I_{AB}) = 28$ and $\mu(B_{AB}) = 29$ mag arcsec⁻² level, respectively, with the important proviso that the isophotal diameter was not allowed to shrink below 2".0.

2.4. Object Detection and the Generation of a Statistically Complete Catalog

Two independent image-detection algorithms were used by two of the authors to generate independent catalogs of detected objects from the two sets of independently reduced images (see above). In each field, detected objects were ranked according to their isophotal I_{AB} magnitudes. Careful comparison of the two catalogs showed good agreement, with differences in ranking reflecting only the statistical uncertainties in magnitudes expected from the independent reductions. Astrometric calibration of the images was undertaken using shallow wide-field images (6' × 6') of the areas surrounding the SSA fields, on which many of the brighter objects in the deep area could be seen along with many stars visible on the Palomar Observatory Sky Survey. The positions of the latter were measured relative to AGK3 stars on glass copies of the POSS at the Royal Observatory Edinburgh.

The *I* band was chosen as the wave band in which to select the primary sample, since it was the longest available wavelength. This has the operational advantage of reducing the effect of differential *K*-corrections at low to moderate redshifts, since $\lambda_{\text{rest}} > 4000$ Å for $z \leq 1$. It also ties the selection of the sample to the oldest and slowest evolving stellar populations within the galaxies. Blue-selected samples, in contrast, are increasingly sensitive to star formation as the redshift increases. For possible objects at high redshift, $z > 1$, choice of the *I* band extends the sensitivity to very high redshifts, since Lyman- α will pass through the *I* band only at $z \geq 5$.

Because of their usefulness as the basis for spectroscopic studies and other investigations, we list in Tables 2A, 2B, and 2C the objects with isophotal $I_{AB} \leq 24.5$ in each field. This sample represents the brightest 100 or so objects in our combined fields and has an average surface density of approximately 8×10^4 deg⁻². This magnitude level represents a 4 σ detection in our 3" aperture or a 6 σ detection in our minimum isophotal radius of 2". Correspondingly, the colors of these

objects are well determined, and this sample is amenable to the study of individual objects, particularly for the bluer objects which stay bright through to the shorter wavelengths. Object-by-object comparison of the two independent samples generated from the independent data reductions, and simulations involving the addition of artificial objects of known brightness, both suggest that the samples in Table 2 are statistically complete, in the sense that, while random photometric errors may move objects in and out of the sample at the faint end, the total number of objects is roughly preserved and objects have not been systematically lost by the image location algorithm. In Table 2 we list for each object the (*x*, *y*) position on the CCD image (to aid in locating objects on Fig. 1) and its 1950 coordinates, its isophotal I_{AB} magnitude, and its 3" aperture I_{AB} , V_{AB} , B_{AB} , and U'_{AB} magnitudes. The first entry for each field is the position of the field center (CCD coordinates 174, 174) and the 1 σ photometric uncertainties of the aperture photometry.

In Figures 1c, 2c, and 3c, we identify these brighter objects in each field, representing the cataloged $I_{AB} < 24.5$ sample with solid symbols. In general, another 30 or so objects are detected in each field with $24.5 < I < 25.5$, and these are represented by open symbols. The addition of artificial objects suggests that our incompleteness rises through this interval from a negligible value at $I_{AB} = 24.5$ to about 50% at $I_{AB} = 25.5$. This is consistent with the number of new objects observed, if the counts continue to have a constant slope of roughly 0.4 mag⁻¹ (see below). These fainter objects with $24.5 < I_{AB} < 25.5$ have been assigned an SSA identification number but have not been included in Table 2 on account of their incompleteness and, in some cases, large photometric errors. Almost all (95%) of these extra objects are seen in *V* as well as *I*, but some of them are undetectable on the *B* and *U'* images. There are also many faint blue objects with $B > 25.5$ that are not detectable in *I*. In total, it is clear from the contour plots that approximately 100 objects are detectable in each field. The high surface density of these fainter objects is discussed below.

Finally, and motivated primarily by the desire to set up a subsample for which it is feasible to obtain complete and unambiguous spectroscopic identifications with existing facilities, a blue-selected subsample has been defined to have isophotal $B_{AB} \leq 24.1$. A blue-selected sample was chosen for the initial spectroscopic study because spectroscopy of the redder members of an *I*-band-selected sample would be difficult on account of the bright and highly featured sky spectrum at $\lambda > 7000$ Å, and because much of the recent survey spectroscopy has been carried out on blue-selected samples with $B < 21.5$ (Broadhurst, Ellis & Shanks 1988) and $B < 22.5$ (Colless, Ellis, & Taylor 1989a; Colless *et al.* 1989b). Details of this blue-selected sample, which forms the basis of much of our discussion, are given below.

2.5. Photometric Classification

Within the constraints imposed by the photometric uncertainties in each wave band, the *U' B V I* spectral energy distributions (SEDs) defined by the magnitudes in Table 1 can be compared with those of stars and with a range of galaxies as a function of redshift. While a unique best-fitting SED can generally be found, the range of acceptable fits, as defined by a χ^2 statistic, usually covers a range of possible redshifts and Hubble types, depending on the noise in the photometry and the shape of the SED. Photometric estimation of redshifts is rightly regarded with some suspicion, and rather than representing an attempt to obtain a single best fit, this fitting

TABLE 2A
SSA 13 COMPLETE CATALOG OF POSITIONS AND PHOTOMETRY

SSA	CCD		R.A.(1950)	Decl.(1950)	$I_{AB,iso}$	I_{AB}	V_{AB}	B_{AB}	U'_{AB}
	x	y							
13-00.....	174.0	174.0	13 ^h 10 ^m 01 ^s .24	+43°00'32".6	...	26.10	26.86	27.40	26.80
13-01.....	107.5	49.4	13 10 02.55	+43 00 05.0	21.64	22.13	23.36	23.78	25.05
13-02.....	191.9	108.3	13 10 00.88	+43 00 18.0	22.16	22.54	23.48	24.44	26.48
13-03.....	245.8	305.4	13 09 59.82	+43 01 01.7	22.53	23.09	24.13	24.67	25.26
13-04.....	156.8	268.7	13 10 01.58	+43 00 53.6	22.54	22.64	23.12	23.79	24.87
13-05.....	280.2	173.3	13 09 59.14	+43 00 32.4	22.70	22.92	23.87	24.49	25.81
13-06.....	177.3	173.4	13 10 01.17	+43 00 32.5	22.93	23.13	23.58	24.31	26.15
13-07.....	102.5	65.1	13 10 02.65	+43 00 08.5	22.95	23.94	24.87	24.97	26.21
13-08.....	30.7	247.2	13 10 04.08	+43 00 48.8	23.16	23.44	24.17	24.26	25.54
13-09.....	90.8	28.4	13 10 02.88	+43 00 00.4	23.28	23.52	23.96	24.28	24.95
13-10.....	60.2	112.9	13 10 03.49	+43 00 19.1	23.41	23.50	24.42	24.66	26.82
13-11.....	274.4	185.1	13 09 59.25	+43 00 35.0	23.51	23.59	24.57	24.73	25.17
13-12.....	165.5	191.2	13 10 01.41	+43 00 36.4	23.60	23.99	24.30	24.57	25.77
13-13.....	161.5	32.0	13 10 01.48	+43 00 01.2	23.68	23.68	24.48	25.21	25.98
13-14.....	113.0	191.5	13 10 02.45	+43 00 36.5	23.70	23.71	25.22	26.78	-28.72
13-15.....	227.5	146.2	13 10 00.18	+43 00 26.4	23.70	23.81	24.90	25.94	-27.00
13-16.....	115.6	39.4	13 10 02.39	+43 00 02.8	23.73	23.79	24.47	25.38	26.80
13-17.....	250.9	195.0	13 09 59.72	+43 00 37.2	23.76	23.76	24.69	25.06	25.69
13-18.....	198.8	50.2	13 10 00.74	+43 00 05.2	23.76	23.76	24.41	24.30	25.68
13-19.....	158.9	187.0	13 10 01.54	+43 00 35.5	23.76	24.18	24.62	24.89	26.76
13-20.....	147.0	118.4	13 10 01.77	+43 00 20.3	23.87	23.96	23.98	24.46	25.41
13-21.....	146.4	233.9	13 10 01.79	+43 00 45.8	23.91	23.88	23.83	24.07	25.13
13-22.....	28.8	196.4	13 10 04.11	+43 00 37.5	24.07	24.06	24.27	24.33	25.94
13-23.....	100.5	208.4	13 10 02.70	+43 00 40.2	24.08	24.08	25.02	25.12	25.88
13-24.....	289.9	76.1	13 09 58.94	+43 00 10.9	24.19	24.10	25.65	28.09	-27.83
13-25.....	147.7	204.5	13 10 01.76	+43 00 39.3	24.25	24.36	25.11	25.02	26.00
13-26.....	52.8	239.8	13 10 03.64	+43 00 47.2	24.32	24.24	25.24	25.47	-29.78
13-27.....	240.1	198.8	13 09 59.93	+43 00 38.1	24.34	24.77	25.64	26.23	-27.01
13-28.....	251.2	297.2	13 09 59.72	+43 00 59.9	24.36	24.48	25.27	24.68	-26.53
13-29.....	20.1	28.3	13 10 04.28	+43 00 00.3	24.43	24.35	24.64	24.88	25.83
13-30.....	259.8	318.6	13 09 59.55	+43 01 04.6	24.46	24.39	24.59	25.62	28.63

exercise is aimed primarily at excluding various alternative possibilities for each galaxy.

For each object detected in this study, stellar and galactic SEDs were compared with the observed SED. Stellar SEDs were derived from Johnson's (1966) compilation, while galactic SEDs have been based on the compilation of Coleman, Wu, & Weedman (1980), interpolating to give seven galactic species spread between E and Irr. An additional SED representing the very blue galaxy NGC 4449 was also used. A range of redshifts between 0.0 and 1.25 was examined for each object. The SEDs were not evolved in any way, the reasonable assumption being made that evolutionary changes will closely approximate the effect of changing to a different Hubble type. A fit was regarded as acceptable if $\chi^2 \leq 5$.

At bright levels, where the uncertainties in the photometry are small, a very large fraction of the galaxies can be represented by normal galaxies at some redshift $z < 1.25$. In fact, only 4% of the $I_{AB} \leq 24.5$ objects listed in Table 2 are definitely unclassifiable in this way, and these are *all* very blue objects in $(B-I)$. One of these (SSA 22-10) has a sufficiently strong emission-line spectrum (at $z = 0.13$; see below) that the broadband spectral energy distribution is seriously distorted, but this cannot be the explanation for two of the others (SSA 22-16 and SSA 22-24), which are observed to be line-free (see below). The fourth object (SSA 13-21) has not been examined spectroscopically. Of course, a successful fit by a normal galaxy does not rule out a more exotic identification at a different redshift, and many of the bluer galaxies could be unusual objects similar to SSA 22-16 or SSA 22-24.

At faint levels, the photometry is sufficiently noisy that few constraints can be placed on the identification of the galaxy. At brighter magnitudes, however, many possibilities can be ruled out in this way. In particular, a *UBVI* data set is well placed to determine whether a galaxy lies at redshifts above or below $z = 0.5$ because the 4000 Å feature and the Balmer break that occurs between $4000 \text{ \AA} < \lambda < 3650 \text{ \AA}$ moves through the *V* band at $0.4 < z < 0.5$.

2.6. Spectroscopic Observations

As a follow-up to the detection and classification of faint galaxies described above, a program of spectroscopic observations of identified objects has been begun. The aim of this program is to spectroscopically identify as many as possible of the objects listed in Table 2, concentrating initially on the subsample defined to have $B_{AB} \leq 24.1$. To date, we have spectroscopically studied only the SSA 22 field. Spectroscopy of faint galaxies with $B \sim 24$ is both difficult and time-consuming. The principal difficulties are in the positioning of the slit onto the faint galaxy, the flattening of the two-dimensional spectrographic image, and the effective removal of strong night-sky lines.

To minimize these difficulties, it was decided to employ a single long-slit spectroscopic aperture, of width 3" and length about 2'. By splitting the long exposures required for these observations into smaller units and then stepping the target objects along the slit for a considerable distance, it was possible to employ statistical artifact removal and sky-determination techniques that are analogous to the

TABLE 2B
SSA 17 COMPLETE CATALOG OF POSITIONS AND PHOTOMETRY

SSA	CCD		R.A.(1950)	Decl.(1950)	$I_{AB,iso}$	I_{AB}	V_{AB}	B_{AB}	U'_{AB}
	x	y							
17-00.....	174.0	174.0	17 ^h 04 ^m 59 ^s .81	+43°59'34".7	...	26.00	26.29	26.78	26.53
17-01.....	274.8	92.2	17 04 57.88	+43 59 15.8	20.14	20.53	21.62	22.21	22.84
17-02.....	157.3	217.5	17 05 00.09	+43 59 44.3	20.58	20.77	21.16	21.28	21.44
17-03.....	136.0	222.8	17 05 00.51	+43 59 45.7	21.77	22.09	22.52	23.21	24.29
17-04.....	158.3	39.6	17 05 00.28	+43 59 06.0	21.96	22.05	24.20	25.74	29.95
17-05.....	221.8	39.6	17 04 59.01	+43 59 05.1	21.99	22.18	23.02	23.48	23.72
17-06.....	315.7	165.1	17 04 56.97	+43 59 31.0	22.02	22.16	23.84	24.94	26.68
17-07.....	216.9	41.6	17 04 59.10	+43 59 05.6	22.08	22.41	23.76	24.26	24.22
17-08.....	120.5	232.5	17 05 00.81	+43 59 48.0	22.19	22.23	23.87	25.04	28.06
17-09.....	67.2	291.9	17 05 01.81	+44 00 01.5	22.44	22.60	23.39	23.91	24.32
17-10.....	72.5	24.3	17 05 02.02	+43 59 03.8	22.57	22.74	22.85	23.34	23.64
17-11.....	258.2	122.0	17 04 58.18	+43 59 22.4	22.74	23.04	23.29	24.43	24.27
17-12.....	191.4	43.6	17 04 59.61	+43 59 06.4	22.86	22.95	23.63	24.85	-26.81
17-13.....	297.0	251.6	17 04 57.24	+43 59 49.9	22.90	23.69	24.25	24.95	24.40
17-14.....	56.6	186.8	17 05 02.15	+43 59 39.0	22.93	23.06	23.91	23.94	24.08
17-15.....	288.0	184.1	17 04 57.50	+43 59 35.4	23.09	23.13	26.39	28.63	25.49
17-16.....	284.1	28.8	17 04 57.77	+43 59 09.0	23.19	23.25	23.55	24.41	24.65
17-17.....	263.9	303.5	17 04 57.84	+44 00 01.5	23.35	23.44	24.79	26.07	27.77
17-18.....	176.2	139.1	17 04 59.80	+43 59 27.2	23.54	23.68	24.80	26.13	25.95
17-19.....	186.5	247.5	17 04 59.47	+43 59 50.4	23.60	23.57	24.98	26.54	27.84
17-20.....	111.7	308.1	17 05 00.90	+44 00 04.5	23.60	24.45	25.48	-28.88	25.57
17-21.....	288.2	251.4	17 04 57.42	+43 59 49.9	23.61	23.93	24.32	25.12	25.22
17-22.....	156.3	129.5	17 05 00.21	+43 59 25.4	23.69	23.75	25.76	27.12	26.54
17-23.....	168.3	272.8	17 04 59.80	+43 59 56.1	23.77	23.99	25.01	26.57	-27.77
17-24.....	243.6	42.2	17 04 58.47	+43 59 05.4	23.78	24.02	25.87	-28.45	-26.60
17-25.....	306.7	245.2	17 04 57.05	+43 59 48.4	23.79	24.07	25.45	-27.12	27.53
17-26.....	65.0	234.6	17 05 01.92	+43 59 49.2	23.91	24.00	24.45	25.17	24.92
17-27.....	280.4	138.2	17 04 57.71	+43 59 25.6	23.96	24.20	24.49	25.18	25.14
17-28.....	267.2	289.1	17 04 57.80	+43 59 58.3	24.06	24.88	25.15	25.47	26.80
17-29.....	324.6	98.3	17 04 56.87	+43 59 16.4	24.07	24.02	26.41	27.33	-27.20
17-30.....	44.2	145.2	17 05 02.45	+43 59 30.2	24.09	24.09	24.10	24.44	24.50
17-31.....	157.7	70.4	17 05 00.26	+43 59 12.6	24.10	24.10	24.31	25.72	25.63
17-32.....	241.5	166.6	17 04 58.46	+43 59 32.3	24.12	24.12	24.54	25.01	24.70
17-33.....	22.3	120.0	17 05 02.92	+43 59 25.1	24.24	24.54	24.42	26.79	25.47
17-34.....	250.1	47.2	17 04 58.43	+43 59 06.4	24.27	24.27	25.41	25.58	-26.78
17-35.....	89.4	231.8	17 05 01.43	+43 59 48.3	24.37	24.86	25.69	25.40	26.80

sky-flattening procedure that was successfully used for the imaging program. Use of a long-slit aperture forgoes the multiplexing advantage of using a multislit focal-plane mask, but this benefit would in any case have been relatively small given the limited field size (70") of each SSA and the need to have a reasonable amount of blank sky on either side of the object for sky removal. In practice, judicious choice of slit position angles has allowed us to observe several target objects simultaneously with a single slit position. The surface density of fainter galaxies is sufficiently high that many other SSA objects, for which we have photometry, will lie on each slit, allowing us to search for serendipitous identifications of any strong-lined objects. Finally, the portions of the slit extending beyond the central SSA area into the shallow survey area may contain other objects that may be included in a serendipitous way.

Positioning of the slit over the target objects was achieved by means of a rotational offset of the whole Cassegrain environment, so that the slit lay at known position angle about a star that was bright enough to be readily seen on a short field exposure through the spectrograph. After each spectroscopic exposure, the telescope was moved in right ascension and declination so that this star, and the target object(s), moved along the slit by about 10". A number of such exposures were obtained at each slit position angle. After the usual bias sub-

traction and dome flat-field division, a crude sky subtraction was applied, after which a median residual sky frame was constructed. This frame, which represented the effect of chip defects and low-level nonlinearities was subtracted from all frames, after which a more precise sky removal, using a low-order polynomial fit to the sky at a given wavelength, was undertaken. Finally, the images were co-registered by means of the bright star and co-added, with a filter to remove cosmic-ray events.

Three position angles have been observed to date on two runs in 1988 July and 1989 July for total integration times of 20 hr (SSA 22-24), 7 hr (SSA 22-7, 22-10, 22-11, and 22-16) and 2 hr (SSA 1 and SSA 3), respectively. One-dimensional spectra of each object visible on the slit profiles were extracted from the two-dimensional image using an optimized extraction profile. This profile varied as a function of wavelength because of defocusing of the spectrograph at the extremes of the wavelength range. Consequently, in order to preserve the spectrophotometric information, an overall continuum shape was determined from a much wider extraction from the data, and a highly smoothed continuum correction derived from this was applied to the higher S/N spectrum obtained from the optimized extraction.

While many of the faintest spectra were uninterpretable on

TABLE 2C
SSA 22 COMPLETE CATALOG OF POSITIONS AND PHOTOMETRY

SSA	CCD		R.A.(1950)	Decl.(1950)	$I_{AB,iso}$	I_{AB}	V_{AB}	B_{AB}	U'_{AB}
	x	y							
22-00.....	174.0	174.0	22 ^h 15 ^m 01 ^s .00	+00°00'05".8	...	26.00	26.13	26.72	27.00
22-01.....	160.2	142.4	22 15 01.25	-00 00 00.9	19.35	19.60	20.82	22.17	24.78
22-02.....	307.5	332.7	22 14 58.97	+00 00 38.7	20.60	20.66	22.43	23.67	25.80
22-03.....	219.8	192.8	22 15 00.34	+00 00 09.3	20.83	21.00	22.39	23.51	27.62
22-04.....	160.1	217.2	22 15 01.20	+00 00 15.0	21.16	21.24	22.61	23.74	26.77
22-05.....	284.8	20.8	22 14 59.56	-00 00 29.3	21.44	21.57	22.92	24.07	26.07
22-06.....	264.3	283.1	22 14 59.64	+00 00 28.3	22.06	22.20	23.41	24.43	27.71
22-07.....	134.6	39.1	22 15 01.73	-00 00 23.1	22.15	22.22	22.74	23.66	24.08
22-08.....	24.3	256.0	22 15 03.14	+00 00 25.4	22.36	22.50	23.65	24.15	24.18
22-09.....	94.1	252.0	22 15 02.13	+00 00 23.9	22.58	22.67	26.94	26.49	-27.05
22-10.....	30.9	46.0	22 15 03.27	-00 00 20.3	22.62	22.77	22.77	23.37	23.95
22-11.....	192.3	36.1	22 15 00.91	-00 00 24.5	22.63	22.67	24.19	25.24	26.14
22-12.....	117.8	279.4	22 15 01.77	+00 00 29.4	22.77	22.77	23.09	23.61	24.62
22-13.....	78.0	209.6	22 15 02.41	+00 00 14.6	22.79	22.99	24.06	24.33	24.69
22-14.....	207.8	168.3	22 15 00.56	+00 00 04.3	22.87	22.92	23.61	24.18	24.66
22-15.....	286.6	252.6	22 14 59.33	+00 00 21.5	22.89	23.01	25.04	26.85	27.37
22-16.....	51.4	45.9	22 15 02.93	-00 00 20.6	22.92	23.21	23.55	23.62	23.58
22-17.....	185.4	93.5	22 15 00.96	-00 00 12.1	22.93	22.93	23.53	24.05	24.67
22-18.....	230.2	183.5	22 15 00.21	+00 00 06.9	23.04	23.68	24.19	25.22	26.26
22-19.....	303.3	93.0	22 14 59.21	-00 00 13.6	23.24	23.57	24.54	25.73	26.41
22-20.....	19.3	222.3	22 15 03.27	+00 00 18.2	23.42	23.47	25.22	25.14	25.81
22-21.....	236.4	134.5	22 15 00.15	-00 00 03.3	23.57	23.82	24.93	25.28	25.99
22-22.....	330.7	75.3	22 14 58.84	-00 00 17.6	23.81	23.81	28.73	-26.05	28.90
22-23.....	35.2	290.2	22 15 02.97	+00 00 33.3	23.82	24.12	25.44	25.96	26.24
22-24.....	88.8	282.2	22 15 02.20	+00 00 30.5	23.87	23.88	23.78	24.04	25.09
22-25.....	265.4	19.3	22 14 59.85	-00 00 29.1	23.99	23.99	25.30	25.05	25.94
22-26.....	325.0	274.7	22 14 58.77	+00 00 26.1	24.04	24.28	26.02	25.81	27.17
22-27.....	19.1	186.8	22 15 03.30	+00 00 10.3	24.05	23.97	25.04	25.24	26.35
22-28.....	162.8	95.6	22 15 01.29	-00 00 11.1	24.14	24.10	26.38	26.82	-27.29
22-29.....	301.4	229.6	22 14 59.15	+00 00 16.2	24.23	24.18	25.43	26.06	26.46
22-30.....	295.5	74.7	22 14 59.38	-00 00 17.8	24.29	24.24	25.31	26.66	25.68
22-31.....	212.2	242.6	22 15 00.45	+00 00 20.2	24.30	24.23	24.51	25.37	25.52
22-32.....	232.8	102.8	22 15 00.27	-00 00 10.5	24.36	24.33	26.64	-27.65	-28.21
22-33.....	111.5	115.8	22 15 02.00	-00 00 06.1	24.39	24.34	25.60	25.49	27.15
22-34.....	108.9	310.2	22 15 01.89	+00 00 36.8	24.48	24.50	24.91	26.15	25.55
22-35.....	272.5	74.0	22 14 59.71	-00 00 17.5	24.49	24.61	24.87	27.57	-27.68

account of the low S/N, a high success rate was achieved on our primary targets with B -magnitudes as faint as $B \sim 24$. Figure 4 shows the blue-visual slit functions for each position angle with identifications of those objects lying above a certain threshold on the slit function. These objects represent a "complete" sample based on continuum brightness, and all of them were examined in detail. The spectra of the extragalactic objects in the SSA 22 field, plus that of the serendipitous galaxy "Anon A" at $z = 0.53$, are shown in Figure 5, along with line identifications.

Cowie & Lilly (1989) presented a preliminary spectrum of the flat-spectrum galaxy SSA 22-24 based on the first 7 hr of observation (taken in 1988 July) at this slit position angle, and suggested that this object might have $z = 3.4$, based on an emission line and continuum break feature. We were unable to confirm the existence of the emission line in our second (14 hr) observation obtained in 1989 July, and have been unable to determine unambiguously the redshift of this object. Similarly, SSA 22-16, also identified by Cowie et al. (1988) as a flat-spectrum galaxy, has a featureless continuum that has not yielded a redshift. Aside from these two objects, however, we have secure redshifts for four galaxies in the SSA 22 region (SSA 22-01, 22-03, 22-07, and 22-10), and both of the other two galaxies with $B_{AB} < 24.1$ that lay on the slit outside the deeply imaged area.

The implications of these spectroscopic results will be discussed in § 4.

3. THE BASIC FEATURES OF THE IMAGING DATA

In this section, the gross observed features of our photometric data will be discussed and placed within the context of the broadly comparable data set of Tyson (1988). In general, terms, when compared with Tyson's data, our own have more extensive wavelength coverage and better image quality but cover a much smaller area of sky. In § 4 a more detailed interpretation of the data will be made.

3.1. The Color-Magnitude Diagram

One of the most interesting properties of the population of faint galaxies is the pronounced trend, even in an I -band-selected sample, toward bluer colors at fainter magnitudes (e.g., Kron 1980; Koo 1986; Tyson 1988). In Figure 6 we show the $(B-I)_{AB}$ colors of all objects with isophotal $I_{AB} \leq 25.5$ for the three fields and for the combined data set. Objects not detected in B (i.e., those with flux densities less than the 1σ level), were assigned a flux density equal to the $+1 \sigma$ level in calculating the colors. The $(B-I)_{AB}$ colors for these objects are thus low estimates and are represented as open symbols.

Even allowing for the faint red objects with lower limits to $(B-I)_{AB}$, the blueward trend is clearly seen in our data.

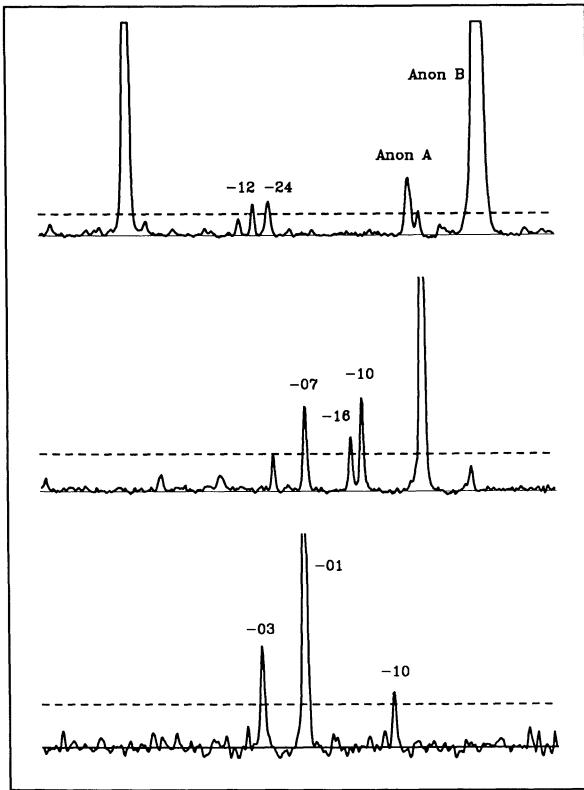


FIG. 4.—Slit function for the deep spectroscopic integrations on the SSA 22 field and surrounding areas. All objects above a certain threshold were examined in detail and are reported on in Table 3.

Although it is an I -band-selected sample, the median $(B-I)_{AB}$ color decreases from 1.9 for objects with $I_{AB} < 22.5$ to 1.2 for $24.5 < I_{AB} < 25.5$. At fainter levels there are several objects which have $(B-I)_{AB} \sim 0$, which implies a flat spectral energy distribution in f_ν . In previous papers we have identified these blue galaxies as “flat-spectrum” galaxies (Cowie et al. 1988), which we have loosely defined to have $(B-I)_{AB} \leq 0.8$. Two points are particularly noteworthy. First, the fraction of flat-spectrum objects increases to fainter magnitudes. Second, we find very few objects with $(B-I)_{AB} < 0.0$, implying that there are few objects that have an f_ν spectral energy distribution that rises to shorter wavelengths, equivalent to having positive α (where $f_\nu = kv^\alpha$). In fact, the few positive- α objects [with $(B-I)_{AB} < 0.0$] that are seen in our data are all consistent with having $(B-I)_{AB} > 0.0$ to within the modest (0.3 mag) photometric uncertainties of the faintest objects.

Figure 6 is most directly comparable to Tyson’s (1988) Figure 16, on which an uncorrected $(B_J - R)$ color is plotted against R over a roughly equivalent magnitude range. In contrast to our own data, his Figure 16 contains large numbers of objects with positive α , with a significant fraction of the objects with $R \sim 26$ having $(B_J - R) \sim -0.7$. This is about 1.0 mag bluer than the colors of a flat f_ν spectral energy distribution and corresponds to $\alpha \sim 2.5$. Indeed, when Tyson applies his statistical corrections to the data to remove “systematics,” the mean $(B_J - R)_{AB}$ color for objects with $24 < R < 25$ is a very blue $(B_J - R)_{AB} \sim 0.1$, while for $25 < R < 26$ his mean color decreases further to $(B_J - R)_{AB} \sim -0.2$ (his Fig. 17), equivalent to the colors of only our very bluest objects.

This substantial difference with Tyson’s data is illustrated in Figure 7, where we plot our mean $(B-I)_{AB}$ colors (in the latter case taking the colors of galaxies undetected in the B band at their lower limits) as a function of isophotal I_{AB} magnitude. Our mean color is roughly constant with magnitude for $I_{AB} > 23$. We have plotted Tyson’s “corrected” mean $(B-I)_{AB}$ colors (derived from his Fig. 17), which show a steady decrease to fainter magnitudes. Although the agreement is fair at brighter magnitudes, by $24.5 < I_{AB} < 25.5$, corresponding to $25 < R < 26$, the discrepancy at the faint end is as large as 0.8 mag.

In summary, whereas Tyson (1988) finds the *general* galaxy population at faint magnitudes to be extremely blue, we find that the *bulk* of the faint galaxy population is actually considerably redder, by almost a magnitude, with only a small number of objects with truly flat spectral energy distributions in f_ν , and essentially none that are significantly bluer than this.

This difference is very significant because it dramatically increases the fraction of galaxies in Tyson’s data that cannot be represented by a normal galaxy spectral energy distribution at any redshift. There is, of course, considerable difficulty in constructing a model stellar population that has a spectral energy distribution with $\alpha \geq 0$ (see, e.g., Bruzual 1983). It is also implausible that strong emission lines could affect the B -magnitudes of enough objects to produce such blue colors in the general population. Consequently, given the robustness of our aperture photometry, we believe that our color distribution (e.g., Fig. 6) is to be preferred over that of Tyson (1988), and that there are actually rather few galaxies that are bluer than flat f_ν , i.e., those which have $\alpha > 0$. We suspect that the problem may have arisen in Tyson’s corrections for “systematics,” noting that his “uncorrected” mean colors lie not far from our own data (which do not require such correction).

3.2. The Number-Magnitude Relation in B and I

The second major phenomenon exhibited by faint galaxies is the steep slope of the number counts. While sub-Euclidean, the counts at faint magnitudes in both B and I bands are significantly above those expected from a nonevolving population of galaxies. Figures 8 and 9 show the B -band and I -band differential number counts derived from our sample compared with nonevolving predictions and Tyson’s (1988) counts. The nonevolving models are those of Yoshii & Takahara (1988). It should be noted that these are normalized with a local estimate of ϕ^* (0.0023 Mpc^{-3}), and no attempt has been made to fit them to the data.

In constructing Figures 8 and 9 from our data, a correction has been applied at the faint end for incompleteness in the detection of objects. This was estimated, as above, by the addition to the images of objects with light profiles derived from other brighter galaxies and of known integrated brightness. This was followed by a reapplication of the image-detection algorithm. We have not continued the counts beyond the point where this incompleteness correction exceeds a factor of 2. The other potential systematic effect, that of underestimating the brightnesses of detected faint galaxies by using an isophotal magnitude measurement, is reduced in our data by our setting a minimum isophotal radius of $2''.0$. Of course, this effect is also mitigated for the faintest galaxies where incompleteness is significant by the fact that it is only the statistically brighter objects that are detected in the first place. Our simulations

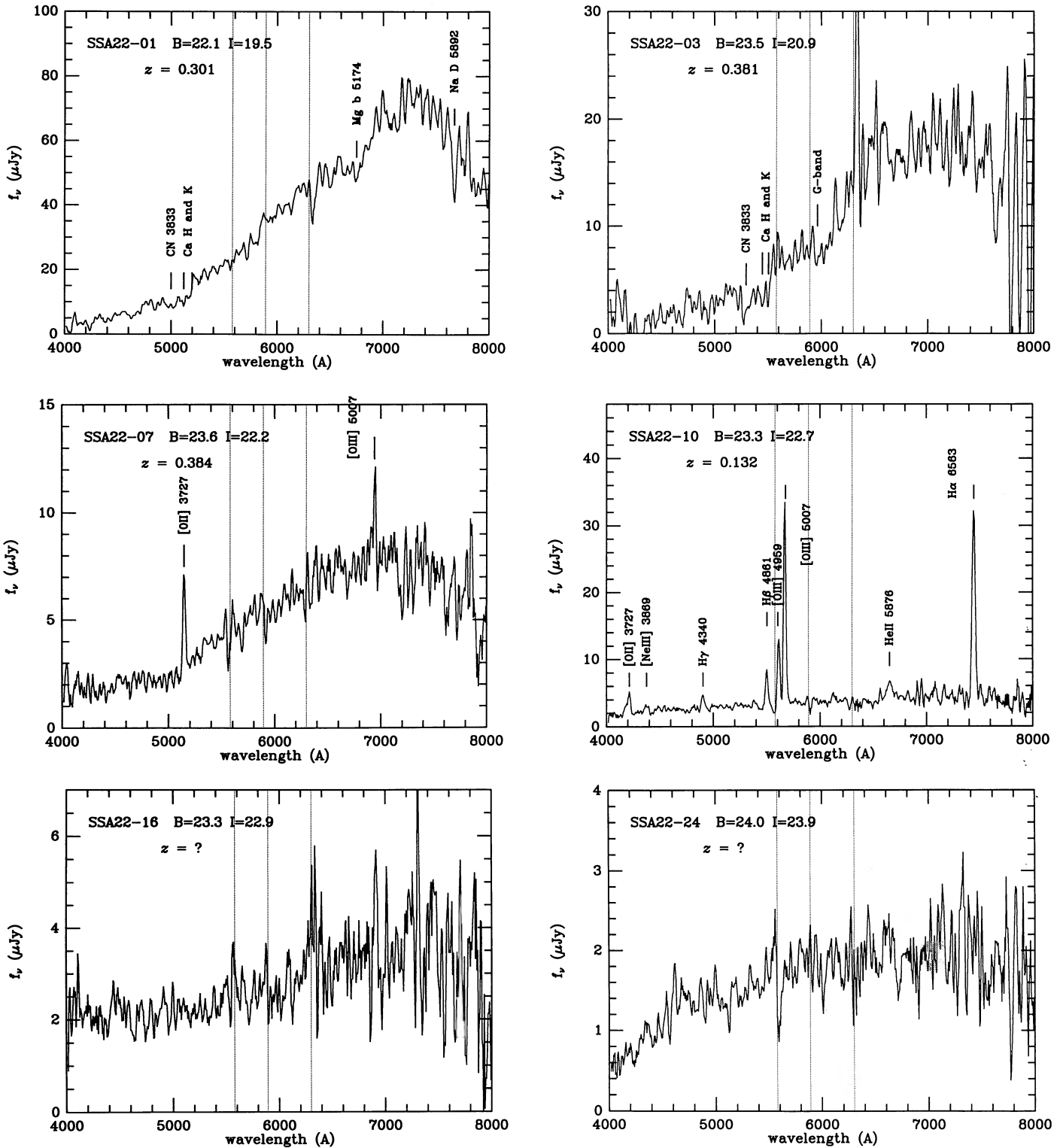


FIG. 5.—Spectra of extragalactic objects observed spectroscopically

suggest that the size of any *systematic* offset in the magnitudes of *detected* objects is small (≤ 0.2 mag) over the whole magnitude range.

Comparison between different number count observations and between them and model predictions are considerably more difficult than with colors, for which close agreement

should be expected. Ellis (1983) has reviewed the dispersion in different estimates of the number counts at brighter levels. To within a similar tolerance, there is broad general agreement between our counts and the uncorrected counts of Tyson (1988). Nevertheless, our corrected counts in the *B* band are not as high at the faint end as those of Tyson, although the

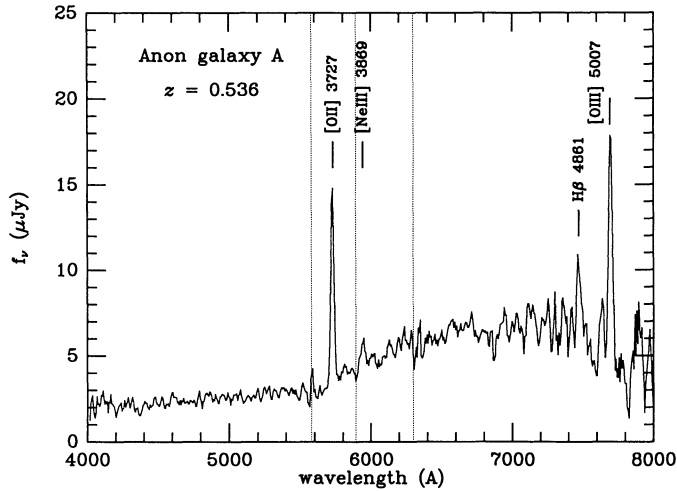


FIG. 5.—Continued

uncorrected counts agree well. On the other hand, in the I band there is better agreement between the final corrected counts than between the uncorrected ones!

Our counts at the faint end, $AB > 23.5$, are well represented by straight power laws with spectral indices of about 0.38 in B and 0.32 in I , which may be compared with 0.45 and 0.34 in Tyson's data. A discrepancy in slopes between Tyson's and our own data at the faint end is to be expected given the roughly 0.8 mag difference in mean $(B-I)$ color of the faintest galaxies which we discussed above. A reduction in slope of the B -band counts below 0.4, as indicated by our data, has the minor but attractive feature of eliminating the potential divergence of the integrated sky brightness. It also brings the B -band counts onto a track that runs more nearly parallel to the nonevolving model predictions. It should be noted that both data sets show an undercount at the bright end that is caused by the selection of survey fields that were devoid of objects on the Palomar Sky Survey. We suspect that the large corrections applied to Tyson's data (a multiplicative factor of 2.5 even at $B_{AB} \sim 26$) may be the source of those discrepancies which are seen. In the broadest sense, both data sets agree with earlier evidence that there is a substantial excess of galaxies at faint magnitudes over nonevolving predictions in both wave bands. This effect is larger at the short wavelengths, and at $B_{AB} \sim 26$ the excess

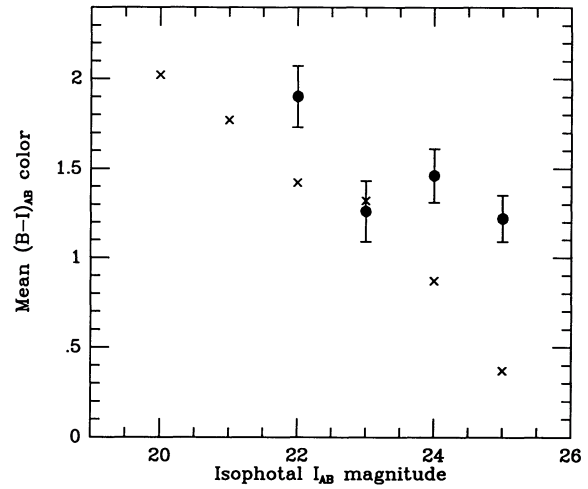


FIG. 7.—Mean $(B-I)_{AB}$ colors of galaxies in the present work (filled symbols) and in Tyson (1988) (crosses) as a function of I -magnitude. Errors on the filled symbols have been calculated as the standard deviation divided by the square root of the number of objects. Statistical errors in the larger sample of Tyson (1988) are much smaller.

relative to the Yoshii & Takahara (1988) models is, in our data, a factor of between 4 and 8, while at $I_{AB} \sim 25$ it is between 2 and 4. We explore this phenomenon in more detail later.

3.3. Sizes of Faint Galaxy Images

The image profiles of faint galaxies are interesting for two reasons. First, they may give information on the spatial distribution of star formation activity which can provide information on the evolutionary state of the galaxies (see, e.g., Baron & White 1987). Second, there are important methodological considerations concerning the possibility of being confusion-limited by overlapping galaxies at very faint levels (see, e.g., Tyson 1988).

In comparison with the data of Tyson (1988), the data presented here are of greatly superior image quality because of the better seeing encountered on Mauna Kea and the smaller projected pixel sampling of the original data, and because no additional smoothing operations have been applied, except to correct for the different seeing of the images in different wave bands in the construction of the accurate aperture colors. Typi-

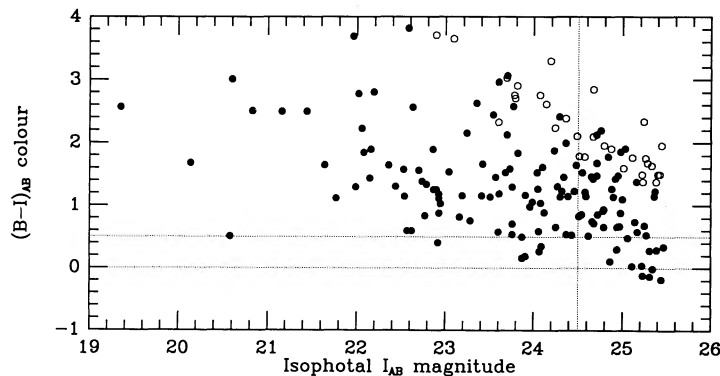


FIG. 6.— $(B-I)_{AB}$ colors of objects with $I_{AB} < 25.5$. Sample is complete to $I_{AB} \sim 24.5$ (vertical line) and suffers approximately twofold incompleteness at $I_{AB} \sim 25.5$. Horizontal line at $(B-I)_{AB} = 0.0$ indicates colors of a spectral energy distribution that is flat in f_{λ} . Open symbols represent objects with only upper limits to the B -band flux. Without exception these objects were detected on the V -band images, and are hence real.

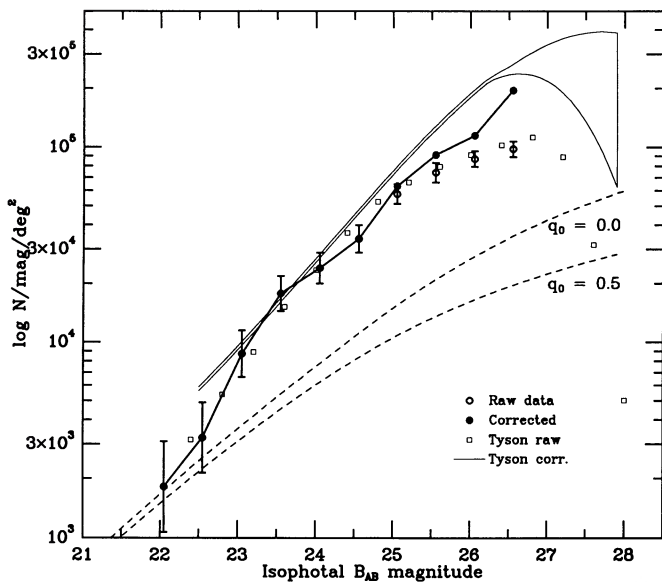


FIG. 8.—Number counts in the B band, uncorrected for stellar contamination, which is negligible for $B_{AB} > 23$. Heavy symbols represent the present data, with the continuous line between filled symbols indicating the expected curve after a correction for incompleteness is applied at the faint end. Open squares and curved locus represent equivalent data from Tyson (1988). The dashed curves indicate a prediction for a nonevolving population of galaxies from Yoshii & Takahara (1988). The steepness of the counts at $B < 23$ is caused mainly by the selection of fields that are empty on the Palomar Sky Survey plates, and the apparent agreement of the observed counts at $B \sim 22$ with the Yoshii & Takahara (1988) nonevolving predictions is coincidental.

cally, the FWHM of stars in the final images is $1''$ or less, with the worst around $1.2''$, in comparison with the roughly $2''$ FWHM of Tyson's (1988) final images. Despite having as high a surface density of images (see Figs. 8 and 9), the images of our fields (Figs. 1, 2, and 3) give the impression of being considerably less crowded than those of Tyson (1988). This is primarily because of the compact cores seen in the vast majority of objects in our images.

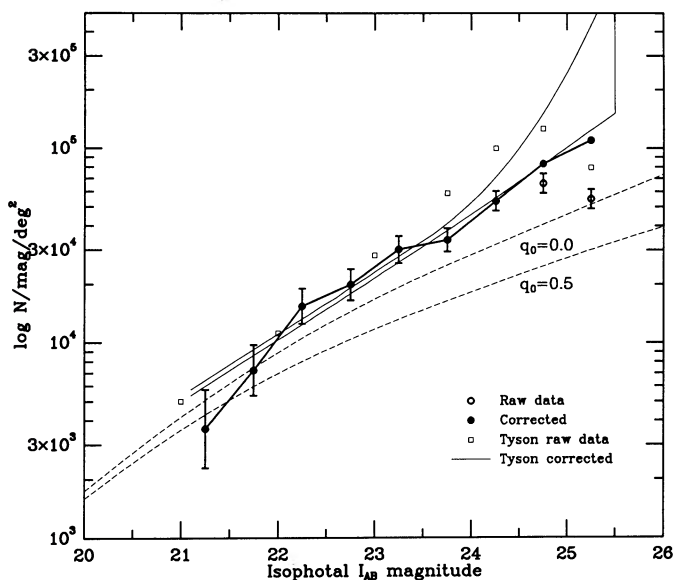


FIG. 9.—Number counts in the I band, uncorrected for stellar contamination. Symbols and lines are as in Fig. 8.

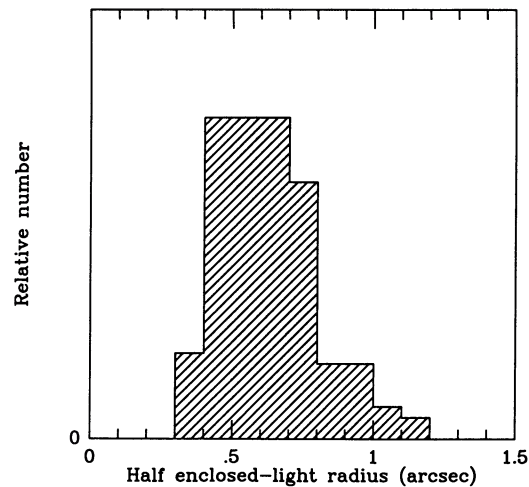


FIG. 10.—Distribution of half-enclosed light radius for all 140 galaxies with $V < 26.5$.

Our best seeing images were generally in the V band, so V -band light profiles were extracted for the 140 objects in the $I_{AB} < 25.5$ sample that had $V \leq 26.5$. These objects have an overall surface density of $1.3 \times 10^5 \text{ deg}^{-2}$ or 36 arcmin^{-2} . The distribution of half-light radii (defined as the radius enclosing half of the total light) for these objects (with no deconvolution) is shown in Figure 10. It should be noted that for Gaussian profiles, $r_{0.5}$ is close to the HWHM of the surface brightness profile. It is clear that the bulk of objects have $0.5 < r_{0.5} < 0.8$. These range from a small number of unresolved Galactic stars to a variety of only moderately resolved galactic images. Indeed, half of the light from the faint galaxy population down to $V_{AB} \leq 26.5$ is coming from only 1.3% of the surface area of the sky on our images, even though the isophotal areas (defined to be at $\mu_{AB} = 28$ in the I band) of these same galaxies cover 12% of the sky (cf. Tyson 1988). Similarly, if the I -band images are simply smoothed to $2''$ resolution, then we find that about 13% of the sky has $\mu_{AB} \leq 28$. Nevertheless, the majority of the objects seen in these smoothed images have central cores that have a surface brightness at least 2.5 mag brighter.

Values of $r_{0.5}$ of around $0.5''$ for the undeconvolved images of faint galaxies are entirely reasonable, since this corresponds to a physical radius of order 5 kpc for objects at cosmological redshifts. Consequently, although a significant fraction of the galaxies overlap at their outermost isophotes, image detections and subsequent photometry from images with $1''$ image quality should not be seriously affected by confusion until the surface densities of objects become substantially higher. The compactness of images in subarcsecond seeing also suggests that high-resolution studies of faint galaxies with the *Hubble Space Telescope* may eventually be rewarding.

4. DISCUSSION

There are currently three major and probably interrelated questions concerning the population of faint galaxies that can be addressed by our imaging and spectroscopic survey. The first concerns the nature of the galaxies at relatively bright magnitudes, e.g., $B \sim 24$, where the number counts are already in excess of nonevolving predictions by factors of 3 or more. These galaxies are sufficiently bright that accurate multicolor photometry and/or spectroscopy can be brought to bear, and yet they are still almost 2 mag fainter than the deepest large-

scale spectroscopic survey yet undertaken (that of Colless et al. 1989b). Second, there is the question of the flat-spectrum galaxies which constitute a significant fraction of the counts for $B \geq 23$. Cowie et al. (1988) have argued in a model-independent way that this population must be responsible for the production of a significant fraction of the presently observed metals in the universe. They appear to be playing a significant role in the processes of galaxy formation and/or evolution, yet their nature remains unclear. Finally, there is considerable interest in the very faintest galaxies seen at $B_{AB} \sim 26$ or $I_{AB} \sim 25$, on account of their very high surface density on the sky. In this section our interpretation of the results of this work will center on these three issues.

4.1. The Nature of 24th Magnitude Galaxies

At $B_{AB} \sim 24$, the number counts of faint galaxies are in excess of nonevolving predictions by factors of 3–4 (Fig. 8). In studies of the number counts with a larger dynamic range than the present one, there is general agreement that the slope of the B -band counts is roughly 0.465 over a wide range of magnitudes, $18 < B < 24$ (see Ellis 1990 for a review). Until the advent of sensitive spectroscopic surveys, this excess was generally thought to represent one or more of the following three effects: (1) an upturn in the local galaxy luminosity function at very low luminosities, resulting in a large number of very low redshift objects; (2) a moderate evolution in luminosity of all galaxies, producing a strong effective density enhancement in above- L^* luminosities and resulting in a greatly enhanced tail in the redshift distribution at $0.5 < z < 1$; or (3) the appearance of a “primeval” population of galaxies undergoing a violent starburst, producing luminous galaxies at the appropriate redshift.

At brighter magnitudes, where the excess is of course considerably smaller than it is at $B \sim 24$, recent spectroscopic surveys of large samples of galaxies to $B < 21.5$ by Broadhurst et al. (1988) and to $B < 22.5$ by Colless et al. (1989a, b) have shown that the redshift distributions of the samples are very similar to the nonevolving model prediction. The mean redshift for $20.5 < B < 21.5$ is 0.22, and for $21.5 < B < 22.5$ it is 0.32. In both studies, no significant high-redshift tail at $z > 0.6$ was seen. This implies that the excess galaxies have the B -band luminosity of roughly L^* galaxies and that the luminosity of above- L^* galaxies cannot have changed substantially since $z \sim 0.6$. This latter conclusion arises because the steep slope of the luminosity function brighter than L^* would produce a large increase in apparent comoving densities for modest enhancements in luminosity. The increased number of sources around L^* was interpreted by Broadhurst et al. (1988) as being caused by bursts of star formation in low-mass systems boosting their luminosities up to approximately L^* levels.

4.1.1. Redshift Distribution at $B = 24$

At $B \sim 24$, the counts are more discrepant. In our deep sample, galaxies with $B \sim 24$ have well-defined colors, allowing us to place some constraints on their redshifts. In addition, it is also possible to obtain spectroscopic redshifts at this level, although this has not been attempted in a systematic way before the present work. We have therefore defined a sample of 22 objects with $B_{AB} < 24.1$ from Table 2. These sources are listed in Table 4. Of these, three objects (all in the low Galactic latitude 22^h field) are stars (two M stars and an F star), and we do not consider them further. The objects in this $B_{AB} < 24.1$

TABLE 3
SUMMARY OF SPECTROSCOPIC OBSERVATIONS ON 22^h FIELD

Name	B	z	EW([O II] λ 3727)
SSA 22-01	22.1	0.301	< 8
SSA 22-03	23.5	0.381	< 8
SSA 22-07	23.6	0.384	35
SSA 22-10	23.3	0.132	85
SSA 22-12	23.6	G star	...
SSA 22-16	23.3	Unidentified	...
SSA 22-24	24.0	Unidentified	...
Anon A	23.1	0.536	61
Anon B	20.9	0.247	?

sample which lie in the 22^h field formed the basis of our initial spectroscopic observations.

While this sample is very limited in number, the wide range of redshifts found in the 22^h field spectroscopy (Table 3) suggests that these objects are to a large degree independent, even in a single field, and that small-scale clustering does not play a major role in distorting the redshift distribution. Hence the statistical *uncertainties* involved in a sample of 22 objects (of order 20%) are comparable to the present *incompleteness* in redshift determinations both in this work and in the brighter spectroscopic surveys (see, e.g., Colless et al. 1989b). In Table 4 we indicate the best-fitting SED and the range of redshifts found in acceptable fits for each object, together, in the case of the 22^h field sources, with the measured redshift from Table 3.

Three points are evident in Table 4. First, the measured redshifts, where they are available, are in remarkably good agreement with the photometrically estimated redshifts. The only discrepancy is the “flat-spectrum” galaxy SSA 22-10, which could not be classified photometrically (see, e.g., Cowie et al. 1988) and yet was found to have the spectrum of an extragalactic H II region spectrum at $z \sim 0.13$. This object has such strong emission lines [EW(5007) \sim 300 Å] that its B and V -magnitudes were significantly distorted, and an acceptable fit is obtained to the continuum (see Fig. 18 below). Second, the only two sources which were observed spectroscopically but for which a redshift was not secured were objects which also could not be *photometrically* classified as normal galaxies (E through to NGC 4449) in the redshift range $0.0 < z < 1.25$. Both of these are examples of “flat-spectrum” galaxies, and, along with SSA 22-10, were identified as such by Cowie et al. (1988). We can be confident in these cases that the difficulty in photometric classification is *not* due to the presence of strong emission lines. Finally, the photometric classifier appears to be relatively effective, as expected, in constraining objects to have $z < 0.5$, with relatively few objects having a range of possible redshifts that significantly span this point. In Figure 11 we compare the distribution of the best-fit photometrically estimated redshifts of the $B_{AB} < 24.1$ sample with the distribution of measured redshifts in the SSA 22 subsample. In a Kolmogorov-Smirnov statistical test, these are consistent at the 30% level (meaning that there is only a 30% chance that they are not drawn from the same distribution), consistent with the assertions that our spectroscopic sample is unbiased and that the photometrically estimated redshifts are a reasonable estimate of the redshifts of the objects.

The redshifts of the $B_{AB} < 24.1$ objects, either measured or estimated, in Table 4 are generally quite modest. Even if the three unclassifiable objects are all assigned arbitrarily high redshifts, the median redshift in Table 4 is 0.38, which is essentially

TABLE 4
SUMMARY OF $B_{AB} < 24.1$ SUBSAMPLE

NAME	B_{AB}	PHOTOMETRIC CLASSIFICATION			SPECTROSCOPY	
		Best-Fit Type	Best-Fit z	Range of z	Type	z
SSA 13-01	23.29	Sc	0.40	0.00–0.42
SSA 13-02	24.06	Sa	0.18	0.04–0.37
SSA 13-04	23.69	Scd	0.19	0.00–0.34
SSA 13-08	23.98	Sc	0.00	0.00–0.20
SSA 13-21	24.09	a
SSA 17-01	21.82	Scd	0.56	0.40–0.75
SSA 17-02	21.09	N4449	0.61	0.27–1.22
SSA 17-03	22.89	Scd	0.20	0.40–0.75
SSA 17-05	23.29	Irr	0.60	0.36–1.22
SSA 17-07	23.93	Scd	0.90	0.78–1.10
SSA 17-09	23.75	Irr	0.40	0.28–0.67
SSA 17-10	23.17	N4449	0.35	0.19–0.51
SSA 17-14	23.81	Irr	1.17	0.93–1.20
SSA 22-01	21.92	E	0.27	0.23–0.42	E	0.30
SSA 22-02	23.61	b
SSA 22-03	23.34	E	0.35	0.31–0.40	E	0.38
SSA 22-04	23.66	b
SSA 22-05	23.94	Sb	0.42	0.13–0.54
SSA 22-07	23.59	Irr	0.39	0.34–0.48	Irr	0.38
SSA 22-08	24.01	Irr	0.71	0.60–0.92
SSA 22-10	23.22	a	H II	0.13
SSA 22-12	23.61	c
SSA 22-16	23.33	a	d	...
SSA 22-17	24.05	Irr	0.31	0.03–0.55
SSA 22-24	24.03	a	d	...

^a Unclassified flat spectrum.

^b M star.

^c F star.

^d Unidentified.

the same as the measured median redshift of the unbiased spectroscopic measurements in Table 3.

The dominance at these magnitudes of relatively low-redshift galaxies at $z \sim 0.4$ can also be seen on two-color diagrams. Figure 12 shows the $(U-B)_{AB}$ versus $(V-I)_{AB}$ two-color diagram for all objects with $B_{AB} < 24.5$. Known stars are represented by star symbols, and objects with $B_{AB} < 24.1$ as larger symbols. Objects which could not be photometrically classified (SSA 22-16, 22-24, and 13-21) are represented as open symbols. Figure 13 is a similar plot in which an overall color, $0.5(U+B-V-I)_{AB}$, and a parameterization of the curvature of the SED, $0.5(U-B-V+I)_{AB}$ (following Koo 1986), are plotted. On both diagrams, the locus of the main-sequence and straight power-law SED colors have been plotted, along with the envelope defined by galaxies of different Hubble type as a function of redshift. In both diagrams it can be seen that the modeled colors of galaxies at $z \sim 0.5$ are moving rapidly across the diagram, and that the location of galaxies on this diagram offers an effective diagnostic of whether they lie above or below $z \sim 0.5$. In each diagram it is apparent that the bulk of the objects lie on the low-redshift side of the $z \sim 0.5$ locus, particularly for the blue-selected $B_{AB} < 24.1$ sample. This is in agreement with the more limited spectroscopic results (Table 3) and detailed SED-fitting analysis above. The I -selected sample contains a number of faint red objects that populate the $z > 0.5$ region of each diagram, albeit with large photometric errors.

Taken together, our spectroscopic and photometric data on the $B_{AB} < 24.1$ sample strongly suggest that this sample is dominated by moderate-luminosity galaxies at modest redshifts. The median redshift is probably close to $z = 0.4$, while

the fraction of very high redshift ($z > 1$) objects is unlikely to be much higher than 20%. This minority blue population will be the subject of § 4.2. In the meantime, we will address the evolution of normal galaxies at $B = 24$, which clearly comprise the bulk of the population.

4.1.2. The Nonevolving Slope of the Source Counts

There has been considerable discussion in the literature of the predicted slope, γ_{NE} , of the number-magnitude source counts for nonevolving galaxy populations in the observed B band (see, e.g., Ellis 1990 for a review). It is in principle straightforward to make this prediction on the basis of the local galaxy population, which can then be replicated to arbitrarily high redshift. Nevertheless, uncertainties in the relative luminosity functions of galaxies of different Hubble type and in the far-ultraviolet spectral energy distributions that should be assigned to each galaxy class have yielded significantly different estimates of this slope. For instance, Broadhurst et al. (1988) derived $\gamma_{NE} = 0.32$ from two independent methods, while Koo & Szalay (1984) derive $\gamma_{NE} = 0.40$. When continued over the several magnitudes over which the number counts can now be followed, this uncertainty results in a significant difference as to the number of galaxies predicted at faint magnitudes.

The present data offer the possibility of an alternative approach, namely, that of “back-counting,” or constructing the nonevolving counts from the observed *faint* galaxy population. This methodology fixes the count at the faint end, with the brighter counts then being constructed from “bringing in” members of the population seen at the higher redshifts. Of

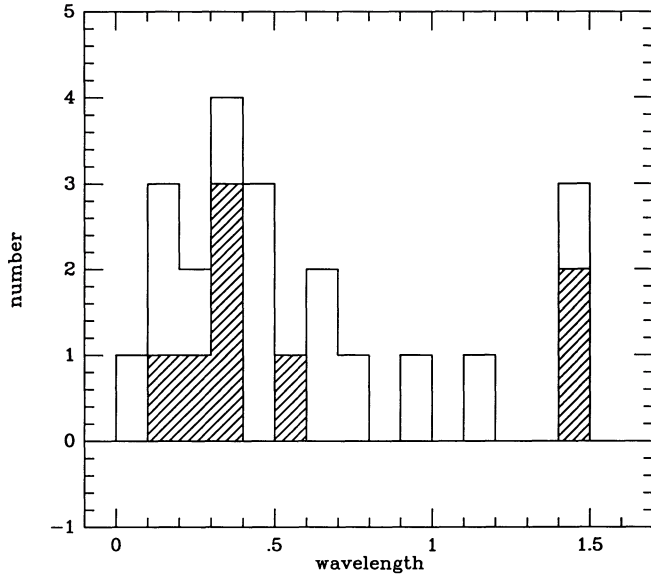


FIG. 11.—Distribution of spectroscopically determined redshifts for an unbiased sample of objects with $B_{AB} < 24.1$ in or around the SSA 22 field (*hatched histogram*) superposed on the distribution of photometrically estimated redshifts for all objects with $B_{AB} < 24.1$ from all three fields (*open histogram*). Objects at $z \sim 1.4$ are those which could not be classified spectroscopically or photometrically. The distributions are consistent at the 30% level.

course, this new approach would only produce the same result as the previous one if the galaxy population were truly not evolving, and this new method should be seen as a complementary approach to the problem. However, the back-counting

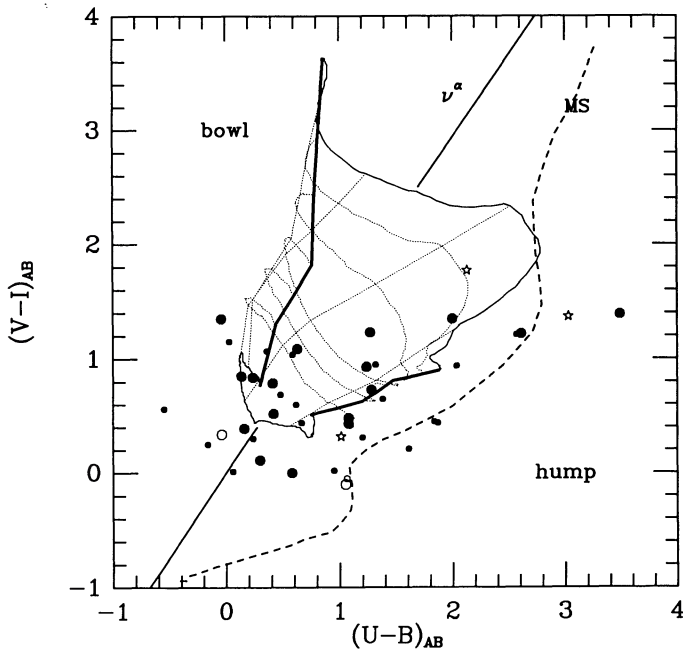


FIG. 12.— $(U-B)_{AB}/(V-I)_{AB}$ two-color diagram for objects with $B_{AB} < 24.5$ (smaller symbols have $24.1 < B_{AB} < 24.5$). Stars represent objects with stellar profiles that cannot be photometrically matched by galaxies at any redshift. Open circles represent objects that cannot be matched with stars of galaxies at $z < 1.2$. The loci of the main sequence and of power-law spectral energy distributions are marked. The mesh of lines represents the envelope of galaxies of varying Hubble type (E to NGC 4449, *top to bottom*) as a function of redshift (0.0, 0.25, 0.5, 0.75, 1.0, and 1.2, *right to left*).

technique avoids the basic uncertainty of unknown K -corrections, since each member of the sample has a well-defined spectral energy distribution for all wavelengths of interest longer than the observed B -band, and furthermore the mix of galaxies is also accounted for in a natural and direct way. It therefore tests the hypothesis that the apparently discrepant number counts may have been caused by a serious error in constructing the local galaxy population.

In view of the limited number of objects in our sample, this analysis has been carried out in a nonparametric fashion using a derivative of the V/V_{\max} approach. Every galaxy found between $23.1 < B_{AB} < 24.1$ was placed at its "best-fitting" redshift, and its luminosity and intrinsic SED calculated from the $U' B V I$ photometry. The minimum and maximum redshifts that this object could then have while still lying in the $23.1 < B_{AB} < 24.1$ magnitude interval were computed and used to define an available volume, and hence a comoving density, for objects of this class. The number counts were then constructed in the usual way, using the empirically determined spectral energy distribution to generate K -corrections. The unclassifiable objects, which are all blue, flat-spectrum objects, were arbitrarily placed at $z \sim 2$. Ideally of course, the redshifts of all objects should be reliably determined spectroscopically. However, to first order, the result is insensitive to the assumed redshifts of the objects, since the analysis is primarily a *differential* one.

The results of this exercise are shown in Figure 14 for $q_0 = 0$ and $q_0 = 0.5$. For the overall population, the slope between $19.9 < B_{AB} < 20.9$ is found to be $\gamma_{NE} = 0.395$. Placing the unclassifiable galaxies at low redshift, $z = 0.3$, increases the overall γ_{NE} to $\gamma_{NE} = 0.41$.

These values of γ_{NE} derived from the distant galaxy sample are clearly within the range of values derived by others from "redshifting out" plausible local galaxy populations (i.e., "forward-counting"), $0.32 < \gamma_{NE} < 0.40$, and certainly less than

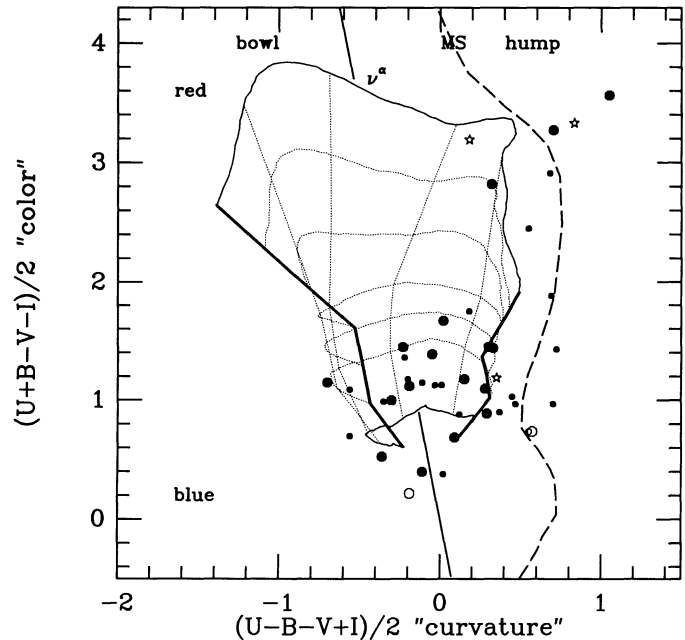


FIG. 13.—Two-color diagram showing an overall color, $0.5(U+B-V-I)_{AB}$ against a measure of the spectral curvature, $0.5(U-B-V+I)_{AB}$. Symbols and lines are as on Fig. 12.

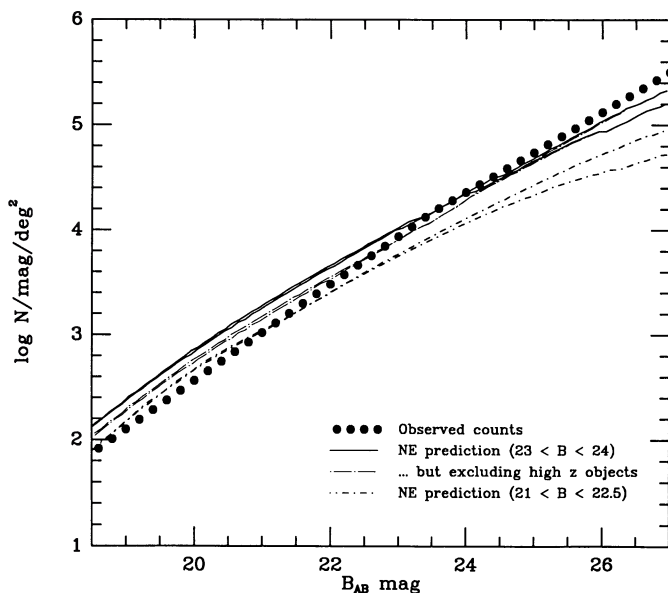


FIG. 14.—Predictions of the number counts in the B band based on non-evolving galaxy populations defined by the observed redshift distributions at $21 < B_{AB} < 22.5$ of Colless et al. (1989b) and $23.1 < B_{AB} < 24.1$ of the present work, compared with the observed counts. The curves also show the effect of placing the unclassifiable objects at low redshift ($z = 0.3$) in the faint sample. See text for details.

the observed slope of $\gamma_{\text{obs}} \sim 0.465$ (Tyson 1988; this work). It should again be stressed that the aim here is not to attempt to discriminate between the different forward-counting γ_{NE} values of Broadhurst et al. (1988) and Koo & Szalay (1984), since any evolutionary change in the galaxy population, such as a different distribution of colors, could alter the derived γ_{NE} as a function of redshift. Rather, the aim is to provide a consistency check by showing directly that the apparent evolution indicated by the discrepancy between γ_{NE} and γ_{obs} is not caused by a straightforward error in determining the *local* galaxy population. The discrepancy between γ_{NE} as determined here and the observed γ_{obs} may be seen in Figure 14, where the non-evolving population defined by the $B \sim 24$ sample overproduces the galaxy counts at $B \sim 18$ by a factor of at least 2.

An important point that should be noted is that, if the observed slope of the number counts is indeed reduced below 0.465 at faint magnitudes (as we have suggested above; but compare with Tyson 1988), then the population defined at $B \sim 24$ can account for the counts at magnitudes fainter than $B \sim 24$ with no further evolution.

A similar analysis based on the much brighter spectroscopic sample of Colless et al. (1989b) at $B < 22.5$ has been carried out. This sample is large (almost 90 galaxies with secure redshifts) but has poorer photometric data, only the $(b_J - r_F)$ colors being available. The roughly 20% of their sample which did not have measured redshifts was ignored, since Colless et al. (1989b) claim that these missing objects should be unbiased in redshift or color with respect to the remainder of their sample, and the total number of objects was normalized to the observed counts at $B_{AB} \sim 21.7$, the mean magnitude of the galaxies in their sample. The less extensive photometric data of this sample mandate a less direct approach to the construction of the galaxy SEDs (see above). The $(b - r)$ colors of our standard galaxy SEDs at the appropriate redshift were used to

assign an SED to each galaxy, interpolating where necessary, and hence to produce K -corrections as a function of z . Our analysis produces a γ_{NE} of about 0.39 over the $20 < B_{AB} < 23$ range, similar to that found above. We have plotted these predictions in Figure 14.

The nonevolving prediction derived from the Colless et al. (1989b) data at $B_{AB} \sim 21.7$ produces a shortfall at $B_{AB} \sim 24$ of a factor of 1.5, emphasizing that substantial changes in the galaxy population are required even over this 2 mag range. This *direct* demonstration is important because the two samples are selected in very similar ways from similar observational material and thus avoid the not inconsiderable difficulties involved in relating the measurements of very bright local samples of galaxies to very faint populations at $B \sim 24$.

Our analysis of the nonevolving counts based on the directly observed high-redshift population therefore confirm the conclusion that the galaxy population at $B \sim 24$ must have undergone significant evolution even when compared with the population defined by the Colless et al. (1989b) sample at $B \sim 21.5$.

4.1.3. General Effects of an Evolving Luminosity Function

At this point we pause to consider in very general terms the effects that evolving luminosity functions will have on the numbers and redshift distributions of faint galaxies.

Regardless of the actual physical processes that are occurring in individual galaxies, the evolution of the galaxy population must be representable in terms of an evolving luminosity function. Indeed, the observational task essentially reduces to defining this time-dependent luminosity function and subsequently interpreting it in terms of physical models for the evolution of individual galaxies. There are, of course, close parallels here to the extensive work on the evolution of the radio source population (see, e.g., Peacock 1985). In this section we consider in general semianalytic terms three generic time-dependent luminosity functions and examine their first-order effects on the faint galaxy counts and on the redshift distributions at faint magnitudes.

We assume that the luminosity function always has a Schechter form of constant faint-end slope and parameterized by simply L^* and ϕ^* , and we examine the effects of changing L^* and ϕ^* . Three simple changes are of particular interest. The first model represents "luminosity evolution" and changes $L^*(\tau)$ with a fixed ϕ^* . This scheme is representative of the classical models of Tinsley (1980), Bruzual (1983), and Yoshii & Takahara (1988). Physically, such evolution would be produced if the luminosity evolution of individual galaxies within a given class of galaxy was independent of their original luminosities and if the number density of galaxies was conserved. An alternative possibility represented by the second model is to have $\phi^*(\tau)$ with fixed L^* . A "density evolution" of this sort does not necessarily require nonconservation of galaxy numbers and could well be produced by an evolutionary scenario of the type suggested by Broadhurst et al. (1988) in which bursts of star formation of a fixed size occur in galaxies. These bursts will have a larger effect on the magnitude of low-luminosity galaxies, and this will cause an effective increase in the numbers of galaxies around L^* . Our third model involves changes in both ϕ^* and L^* whereby an increase in ϕ^* is matched by a decrease in L^* (i.e., the product $\phi^*L^* = \text{constant}$) such that the total brightness of the galaxy population is conserved. This model can be considered representative of the effects of straightforward mergers of galaxies.

It should be stressed that any of these heuristic models could be based on several diverse physical processes. For instance, an apparent evolution in ϕ^* (model 2) could be produced by a combination of L^* evolution (model 1) and merging (model 3). This emphasizes the difficulty of extracting physical information from the observations.

Because the shape of the luminosity function is the same in all these simple representations, the visibility function for the galaxy population within a given apparent magnitude range can be represented, to first order, by a bell curve whose height will be determined by the comoving volume element at the modal redshift and the effective value of ϕ^* and whose width will be roughly constant in $\log z$. The total number of galaxies per magnitude interval is thus given by

$$\log N = \log (dV/dz) + \log z + \log \phi + \text{constant} ,$$

where all quantities are evaluated at the model redshift, z_{mod} . The value of z_{mod} will be set by M^* ($= -2.5 \log L^*$) and the apparent magnitude of the sample in question through the usual relations for luminosity distance and K -corrections. We incorporate these into a $\kappa(z, \lambda, q_0)$ function:

$$\log z_{\text{mod}} = -0.5\kappa(z, \lambda, q_0) \log L^* + \text{constant} .$$

Consequently, the change in $\log N$, $\Delta(\log N)$, and the change in $\log z_{\text{mod}}$, $\Delta(\log z_{\text{mod}})$ are given by

$$\Delta(\log N) = -0.5\kappa \left\{ \frac{d[\log(z dV/dz)]}{d(\log z)} \right\} \Delta(\log L^*) + \Delta(\log \phi^*)$$

and

$$\Delta(\log z_{\text{mod}}) = -0.5\kappa \Delta(\log L^*) .$$

The quantities $d[\log(z dV/dz)]/d(\log z)$ and the geometry/ K -correction term $0.5\kappa(z, \lambda, q_0)$, are tabulated in Table 5 for $z = 0.5$ and $z = 1$, in universes with $q_0 = 0.0$ and $q_0 = 1.0$ (a Euclidean geometry is included also for comparison), for both the B and K bands. In computing K -corrections, we have taken a spectral energy distribution appropriate for an Sbc galaxy (Coleman et al. 1980).

The dependencies of the log number density per magnitude interval ($\log N$) to changes in $\log \phi^*$, in $\log L^*$, and in $\log n$

($= \log \phi^* = -\log L^*$ in the third, merging, scenario) are listed in Table 5 for the different redshifts, cosmologies, and passbands. Finally, in Table 5 we list the relationship between N and $\log z_{\text{mod}}$ for the three models discussed above: (1) $\phi^* = \text{constant}$, (2) $L^* = \text{constant}$, and (3) $\phi^*L^* = \text{constant}$ (where the distinction between the different wave bands has now been dropped because the differences are small).

Several things are apparent in the numbers in Table 5. Most trivially, and as noted above, there is little dependence on wavelength, since the K -corrections for an Sbc galaxy are similar at B and K at the redshifts of interest. Second, and more important, changes in ϕ^* and L^* are both very effective in changing the number of objects per magnitude interval. The former will also have a relatively strong effect on the value of z_{mod} (with z_{mod} roughly going as $N^{0.5}$), but in contrast, z_{mod} is unaffected by changes in ϕ^* . However, when ϕ^* and L^* are coupled in the brightness-conserving merger scenario, it can be seen that there will be little change in N . In other words, straightforward merging in which the overall brightness of the galaxy population is conserved will have only a weak effect on the number of galaxies per unit magnitude interval, particularly in the $q_0 = 0$ case. This is because the slope of the galaxy counts in this model is approximately 0.4. Merging therefore slides the galaxy population up and down the $\log N-m$ relation giving, to first order, little observable effect. In contrast, evolution of either ϕ^* or L^* alone displaces the population from the original relationship, producing a large first-order effect. Since the observed slope of the counts is reasonably close to 0.4 in essentially all wave bands, this result is quite general: merging per se is unlikely to be the cause of the high numbers of faint galaxies seen in the source counts. In fact, since the effect of merging is to stretch the galaxy population up the observed $\log N-m$ relation to fainter magnitudes, the second-order effect (taking into account the changing degree of merging with redshift) will be to *decrease* the number of faint galaxies. It should be noted, however, that merging is effective in reducing the value of z_{mod} without producing a large change in N .

While the assumption that the shape of the luminosity function maintains a constant Schechter form is unlikely to be correct, small perturbations in the luminosity function away from the L^* region will not grossly affect the integrated visibil-

TABLE 5
EFFECTS OF AN EVOLVING LUMINOSITY FUNCTION

PARAMETER	$q_0 = 0$		$q_0 = 0.5$		EUCLIDEAN ALL z
	$z = 0.5$	$z = 1.0$	$z = 0.5$	$z = 1.0$	
$0.5\kappa_B$	0.405	0.375	0.455	0.450	0.500
$0.5\kappa_K$	0.415	0.370	0.465	0.440	0.500
$d[\log(z dV/dz)]/d(\log z)$	2.40	2.17	1.99	1.46	3.00
$\Delta(\log N)/\Delta(\log L_B^*)$	0.98	0.83	0.90	0.65	1.50
$\Delta(\log N)/\Delta(\log L_K^*)$	1.00	0.80	0.93	0.65	1.50
$\Delta(\log N)/\Delta(\log \phi^*)$	1.00	1.00	1.00	1.00	1.00
$[\Delta(\log N)/\Delta(\log n)]_B$	0.03	0.18	0.10	0.35	0.50
$[\Delta(\log N)/\Delta(\log n)]_K$	0.00	0.20	0.08	0.35	0.50
$\Delta(\log z)/\Delta(\log L_B^*)$	0.41	0.38	0.46	0.45	0.50
$\Delta(\log z)/\Delta(\log L_K^*)$	0.42	0.37	0.47	0.44	0.50
$\Delta(\log z)/\Delta(\log \phi^*)$	0.00	0.00	0.00	0.00	0.00
$[\Delta(\log z)/\Delta(\log n)]_B$	0.41	0.38	0.46	0.45	0.50
$[\Delta(\log z)/\Delta(\log n)]_K$	0.42	0.37	0.47	0.44	0.50
(1) $\Delta(\log z)/\Delta(\log N)$	0.42	0.46	0.51	0.68	0.33
(2) $\Delta(\log z)/\Delta(\log N)$	0.00	0.00	0.00	0.00	0.00
(3) $\Delta(\log z)/\Delta(\log N)$	1.85	5.10	1.27	1.00

ity function which is dominated by galaxies around L^* . Furthermore, this analysis clearly excludes the possible effect of strongly evolving young galaxies with very high redshift, and has been concerned only with the effects of the “mild” evolution of the population of “normal” galaxies at “modest” redshifts.

We can summarize the foregoing as follows: Conventional Tinsley-Bruzual-Yoshii/Takehara evolution in L^* produces a change in N , and a corresponding change in z_{mod} (roughly proportional to $N^{0.5}$). An effective evolution in ϕ^* (as could be produced by some bursting evolutionary models) also increases N , but produces no change in the value of z_{mod} . Finally, in a merging model where ϕ^* and L^* are coupled, we would expect little change in N but a reduction in z_{mod} (again roughly proportional to $n^{-0.5}$).

Finally, we can consider the effect of changing the cosmology. Changing from $q_0 = 0.5$ to $q_0 = 0.0$ is to first order equivalent to a change in $\log \phi^*$ and $\log L^*$ of 0.11 and -0.20 , respectively, at $z = 0.5$, and of 0.22 and -0.37 at $z = 1$. These will produce $\Delta(\log N) \sim 2\Delta(\log z)$, but the effects are quite modest, i.e., a change in $\log N$ of only about 0.09 at $z = 0.5$ (as is indeed seen on the curves on Figs. 7 and 8). The corresponding lowering of $\log z_{\text{mod}}$ will be of order 0.04.

4.1.4. Galaxy Evolution at $z = 0.4$

We now return to consider in more detail the redshift distribution for objects in our sample. The modal redshift for an unevolving population of galaxies at $23.1 < B_{\text{AB}} < 24.1$ should be close to $z = 0.4$ (Colless et al. 1989a, b; Yoshii & Takahara 1988) in standard cosmologies. This is remarkably close to that indicated by the present data. Taken at face value, this appears to extend dramatically the results of Broadhurst et al. (1988) at $B \sim 21$ and Colless et al. (1989a, b) at $B \sim 22$, who also found that the redshift distribution matched nonevolutionary prediction, despite the steepness of the number counts and their consequent divergence from the same nonevolving model predictions.

However, some cautionary remarks are warranted. It was shown by Colless et al. (1989a) that simple but representative evolutionary models (chosen to have equal evolution for all Hubble types and luminosities) which fitted the number counts predicted mean redshifts that far exceeded the “no-evolution” prediction. Already by $B = 22.5$, the mean redshift for these models was in excess of $z \sim 0.6$, whereas the mean observed redshift was still at $z \sim 0.3$ (Colless et al. 1989a). By the present level of $B \sim 24$, the mean redshift of the evolving model would be in excess of 0.9, compared with the much lower redshifts found in the present study. However, the use of *mean* redshifts by Colless et al. (1989a) can give a misleading impression. For instance, Yoshii & Takahara (1988, hereafter YT) have published models for evolving galaxy populations that clearly have the bulk of the galaxies at much lower redshifts for similar B -band selected samples, while still accounting for the slope of the galaxy number counts. The discussion of the preceding section suggests that study of the modal redshift may be more illuminating.

In order to look into this question in a more realistic way than was possible in the previous section, we have constructed a suite of simple parametric models that reproduce the features of the YT models and the “straw-man” evolving model of Colless et al. (1989a). For instance, in our program the galaxy mix can be varied between that of Tinsley (1980), which was used by YT, and that of Ellis (1983), which is richer in later

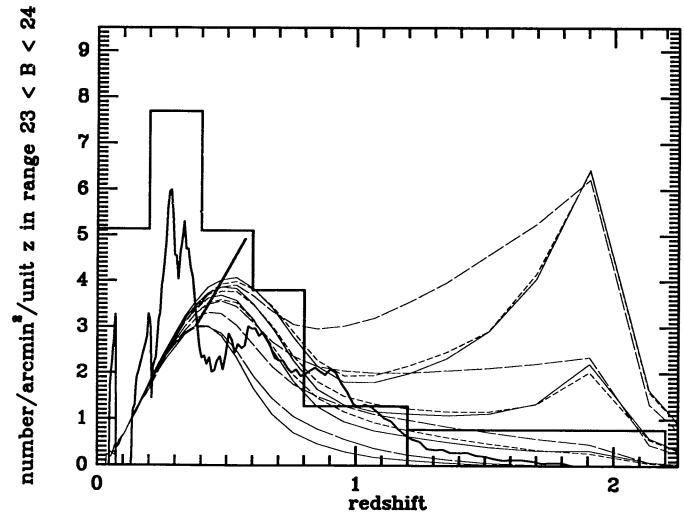


FIG. 15.—Estimated “observed” redshift distribution for the $23.1 < B_{\text{AB}} < 24.1$ subsample compared with predictions based on various formulations of the local galaxy population and the form of galactic evolution (see text for details). These show that the low-redshift $N(z)$ is stable to many of the uncertainties in these formulations, which primarily affect the high-redshift tail. Also shown is the redshift distribution for this magnitude range that is predicted from the faint galaxy $B \sim 21.7$ sample of Colless et al. (1989b), assuming no evolution (see § 4.1.3). These curves stress the apparent increase in comoving space density of the galaxies at $B_{\text{AB}} \sim 24$.

types. We have also parameterized YT’s evolutionary models, which are quite similar to those of Bruzual (1983), for different Hubble types as a function of z and wavelength, and then applied these to the galaxy population according to the prescription of both YT (in which all Hubble types have the “correct” evolution applied) and Colless et al. (1989a) (in which all Hubble types have a uniform evolution applied). In each case, the evolution could be arbitrarily “turned up” by applying a multiplicative factor. Finally, we have taken a ϕ^* of $2.3 \times 10^{-3} \text{ Mpc}^{-3}$ (although the effects of varying ϕ^* are trivially visualized). An important point is that the evolution has been applied independently of the luminosity of the galaxy. This is the classic approach adopted by Tinsley (1980), Bruzual (1983), and, more recently, YT, and was represented in the previous section by model 1.

A large range of these models have been constructed and used to produce predicted redshift distributions for the $23.1 < B_{\text{AB}} < 24.1$ range. These are shown in Figure 15, along with the redshift distribution constructed from the present data (Table 4). As would be expected, the largest variations between the models occur at the highest redshifts where the models are most arbitrary, depending critically on the assumed formation redshift and the details of the formation process. Clearly the *mean* redshifts of these distributions are relatively meaningless.

Of more interest is the distribution of “normal” galaxies at moderate redshifts, $z < 1$. It can be seen that, as expected, the wide range of evolutionary models that have been constructed and plotted on Figure 15 produce a family of similar bell-shaped curves in which there is a close correspondence (for fixed ϕ^*) among the modal redshift, the density of galaxies at that modal redshift (dN/dz) and the width of the distribution. In those models with an evolving L^* , an increase in the total number of galaxies is achieved by adding galaxies at and beyond the modal redshift. As discussed in the previous section, we would expect the density of objects dN/dz at the

modal redshift to be approximately proportional to the modal redshift, z_{mod} , and the total number of galaxies to be proportional to z_{mod}^2 . The line representing dN/dz proportional to $z_{\text{mod}}^{1.2}$ is shown in Figure 15. Clearly, if an increase in dN/dz is required without an increase in the modal redshift, then the "evolution" must be of a form that has the effect of changing the normalization ϕ^* without producing a change in L^* .

If the "observed" distribution of redshifts plotted in Figure 15 is representative of the general population at $23.1 < B_{\text{AB}} < 24.1$, then it is clear that a large effective ϕ^* is required to match this redshift distribution and that luminosity-independent luminosity evolution of all or some part of the galaxy mix is unacceptable. Such evolution increases the number of $0.5 < z < 1$ objects without significantly increasing the number of $0.1 < z < 0.5$ objects, where the excess galaxies are predominantly observed to lie. Clearly an effective value of ϕ^* of order $4.5 \times 10^{-3} \text{ Mpc}^{-3}$ (i.e., twice that used in the models on Fig. 15) is required.

This result is further illustrated when the predicted redshift distribution of the $23.1 < B_{\text{AB}} < 24.1$ sample is produced from the observed redshift distribution of the Colless et al. (1989b) sample, at $20.9 < B_{\text{AB}} < 22.4$ with a mean $B_{\text{AB}} \sim 21.7$, again with the assumption of no evolution in the galaxy population. This is trivially generated by the V/V_{max} analysis of § 4.1.2 and is shown on Figure 15. It emphasizes that the 50% excess in the number counts at $B \sim 23$ relative to the brighter sample is produced by an apparent increase in the number of galaxies at a given redshift rather than by a shift in the redshift distribution to higher redshifts.

The present data therefore appear, within the constraints of our very limited data set, to provide an important extension of the brighter results of Broadhurst et al. (1988) and of Colless et al. (1989a, b). *In effect, the evolution to $B \sim 24$ is primarily manifested as an evolution in ϕ^* .* We should therefore ask what physical effects could be producing this apparent increase in the effective value of ϕ^* ?

In addition to its difficulties in producing the large numbers of excess galaxies at $z \sim 0.4$ (see the previous section), wholesale merging since $z \sim 0.4$ is not very attractive on account of two arguments: First, the general fragility of disks and the observed old ages for disks in galaxies such as our own argues against large-scale merging in massive spiral galaxies over the last several billion years (see, e.g., Ostriker 1990). Recall that the overall number of galaxies needs to be reduced by a factor of 2 or more, so the possible production of ellipticals is quite inadequate. Nevertheless, the galaxies contributing to the excess are of fairly low luminosity ($M_B \sim -19$, about $0.1L^*$) and will have low mass-to-light ratios, since they are generally blue. Whether an L^* disk system such as our own would be destroyed upon consuming such a small galaxy is uncertain. Second, at $B \sim 24$, typical galaxies are still widely separated. Even when seen in projection, the average separation of $B \sim 24$ galaxies on the sky is still about $30''$ (over 300 kpc at $z \sim 0.4$), since there is no strong short-scale spatial clustering of $B \sim 24$ galaxies on our images. Furthermore, nearby objects are not preferentially found to have the same redshifts (see Table 3), so the true separation is correspondingly larger. The excess galaxies are certainly not in the throes of merging at the epoch of observation.

Broadhurst et al. (1988) and later Colless et al. (1989a, b) have advocated a model in which starbursts in low-luminosity, sub- L^* galaxies boost their luminosities up to those of L^* galaxies. Since brighter galaxies are assumed not to take part

in this phenomenon, this process will have the effect of increasing the number of galaxies around L^* , and hence of effectively increasing ϕ^* in a flux-limited sample. Such a model was shown to work in detail for the relatively modest enhancements required at the brighter magnitudes sampled by Broadhurst et al. (1988) and Colless et al. (1989a, b). Nevertheless, because of the flat slope of the Schechter luminosity function at luminosities below ϕ^* , it is quite difficult to achieve substantially larger enhancements in the effective value of ϕ^* , such as would be required at the fainter magnitudes to explain the larger discrepancies in the number counts, and to maintain this for prolonged intervals of cosmic time. For instance, with a standard Schechter function with $M_{B^*} = -21.1$ and $\alpha = 0.1$, it is necessary to integrate down to $M_B = -16$ in order to increase the number of objects brighter than $M_B = -19$ by a factor of 3. A factor of 2 can be accommodated by integrating down to $M_B = -17.5$. Clearly, in this context, it is more difficult to accommodate the required evolution to $z \sim 0.4$ if one starts off with the lower values of $\phi^* \sim 1.4 \times 10^{-3} \text{ Mpc}^{-3}$ found in the southern hemisphere Durham-AAT Redshift Survey (DARS; Efstathiou, Ellis, and Peterson 1988).

Nevertheless, some support for this interpretation comes from the distribution of $(B-I)_{\text{AB}}$ colors in the sample. These are shown, for our galaxies with $23.1 < B_{\text{AB}} < 24.1$, in Figure 16, together with the predictions from nonevolving galaxy population models based on those of YT and of Ellis (1983) (see above). Apart from the extremely blue flat-spectrum galaxies (hatched areas in Fig. 16), which cannot be represented by a normal galaxy spectral energy distribution at any $z < 1.25$, the excess galaxies have the colors of Irr and Scd galaxies at $z \sim 0.4$. The number of red (Sbc and earlier) galaxies is roughly as predicted. This suggests that the excess galaxies are going through an episode of accelerated star formation. We return to consider the limitations of this model when applied to the faintest galaxies at $B_{\text{AB}} \sim 26.5$ in § 4.3.

Another possibility that should be considered is the basic uncertainty in the normalization of the luminosity function, and particularly the effect of the ever larger scale structures

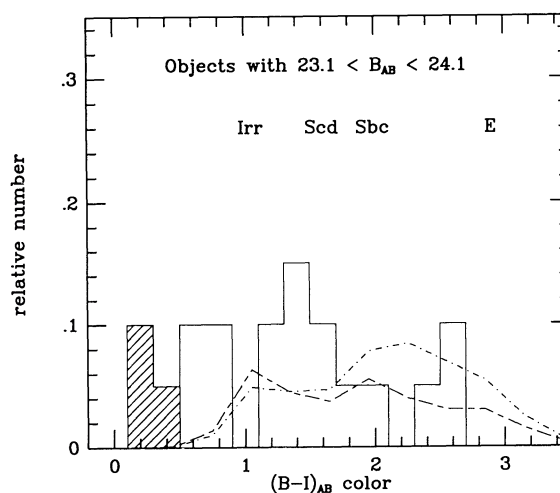


FIG. 16.—Distribution of observed $(B-I)_{\text{AB}}$ color in the $23.1 < B_{\text{AB}} < 24.1$ subsample as compared with the predictions of a nonevolving galaxy population based on the galaxy mixes of Ellis (1983) and Yoshii & Takahara (1988). This shows that the excess of galaxies in this magnitude range have the colors of Scd and Irr galaxies. For reference, the colors of various galaxy types at $z = 0.4$ are shown. Hatched area represents photometrically unclassifiable flat-spectrum galaxies (but excluding SSA 22-10 at $z = 0.13$).

being found in the universe. Of concern here are the well-known discrepancies between different estimates of ϕ^* . As re-analyzed and reviewed by Efstathiou et al. (1988), there are variations of a factor of almost 3 in the value of ϕ^* as measured by different workers, and of 40% between the northern and southern hemisphere measurements by the same group. Some of these problems may be due to large-scale inhomogeneities in the distribution of galaxies. For instance, the “picket-fence” structures seen in the pencil-beam redshift surveys at 21st magnitude (see, e.g., Broadhurst et al. 1990) contain roughly half the galaxies in 10% of the volume, with a characteristic spacing between peaks of order 250 Mpc (for $H_0 = 50 \text{ km s}^{-1} \text{ Mpc}^{-1}$). It should be noted, though, that the deeper redshift surveys such as the DARS (Efstathiou et al. 1988) and the KOSS (Kirshner et al. 1983) extend to high enough redshifts that these particular structures should have been included and their effects averaged out. Furthermore, it should be noted that the Colless et al. (1989b) sample at $B_{AB} \sim 21.7$, relative to which significant evolutionary effects are still seen at $B_{AB} \sim 24.0$, already extends out to median redshift of 0.3! Thus, while it is possible that the galaxy excess is produced by large-scale variations in ϕ^* , such variations must be on very large scales ($z \sim 0.4$).

4.1.5. An Incorrect Cosmological Volume Element?

A more radical alternative is that the faint galaxy counts are telling us that the volume element is not that of a Friedmann-Robertson-Walker metric with $0 < q_0 < 0.5$.

As discussed in § 4.1.3 above, the first-order effect of changing the geometry of the universe is to couple $\Delta(\log \phi^*)$ and $\Delta(\log L^*)$ roughly as $\Delta(\log \phi^*) \sim -1.75 \Delta(\log L^*)$ and to produce $\Delta(\log N) \sim -2 \Delta(\log z)$. A negative value of q_0 would therefore further steepen the counts in all wave bands while slightly decreasing the modal redshift of the sample. As an example of this, we have repeated our construction of the non-evolving number-magnitude counts from the Colless et al. (1989b) data for a flat ($R^{-2} = 0$) and empty ($\Omega_0 = 0$) universe (see, e.g., Peebles 1984). This has a simple exponential expansion and has the $Z_q(z)$ function and comoving volume element of the form

$$Z_q(z) = z, \quad dV_c = (c/H_0)^3 Z_q(z)^2 dz.$$

The nonevolving predictions are shown for the *B*, *I*, and *K* wave bands in Figure 17 for this nonstandard cosmology together with the predictions for Friedmann cosmologies $q_0 = 0.0$ and $q_0 = 0.5$. The infrared observations are taken from Cowie et al. (1990). This model is clearly at least superficially successful at reproducing the number counts in all three bands (particularly when the possibility of mild evolution in the *B* band is included), and will also reproduce a low median redshift in the $23.1 < B_{AB} < 24.1$ sample.

In passing it should be noted that such a cosmology is by no means ruled out by other cosmological tests such as the magnitude-redshift relation. The most extensive Hubble diagram extending to high redshifts is the *K*-*z* relation for powerful radio galaxies (Lilly & Longair 1984; Lilly 1990). A cosmology with negative q_0 would require a larger change in the intrinsic luminosity of the radio galaxies at $z > 1$ compared with local radio galaxies. For $q_0 < 0$ a change of over 1 mag is required (see, e.g., Lilly & Longair 1984; Lilly 1989). While it is easy enough to envisage such strong evolution, it is counter to the “no-evolution” scenario adopted in this discussion. Nevertheless, it could easily be imagined, given the extreme selection

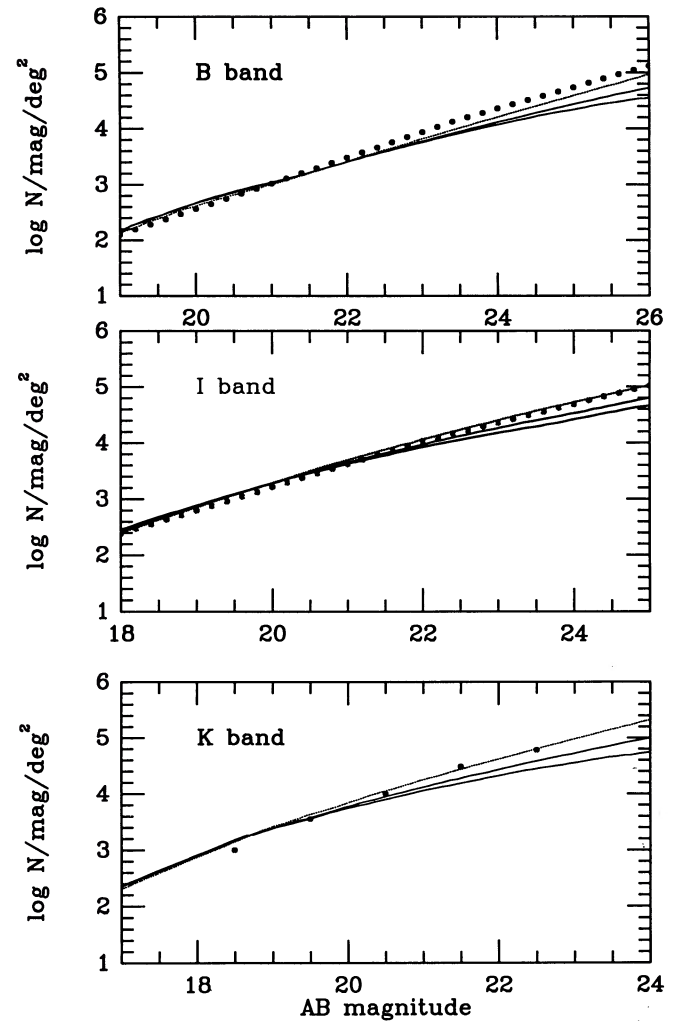


FIG. 17.—Predictions of the number counts in *B*, *I*, and *K* based on a nonevolving galaxy population defined by the Colless et al. (1989b) sample at $B_{AB} \sim 21.7$, for $q_0 = 0.5$ (lowest curve), $q_0 = 0.0$ (middle curve), and a spatially flat geometry with $q_0 = -1$ (upper curve).

biases that may be present in the high-redshift samples, that the evolution of the radio galaxies might be atypical, or that the observed luminosity change was not an evolutionary effect of the stellar populations at all.

In fact, by allowing only very little galaxy evolution, the infrared number-magnitude counts provide the tightest constraints on such nonstandard models. A more lengthy discussion of the pros and cons of these nonstandard models will be presented elsewhere.

4.1.6. Other Possibilities: Disappearing Galaxies

Alternatively, we may be seeing a number of galaxies that are not being counted in local galaxy luminosity functions because they have completely “disappeared” or at least fail to satisfy surface brightness selection criteria for nearby galaxy samples. This would be an extreme version of the Broadhurst et al. (1988) bursting scenario. A large population of very low luminosity dwarf ellipticals might be a plausible product of these galaxies seen at $z = 0.4$. Arguing against this idea is the unexceptional appearance of these galaxies in terms of their morphologies, luminosities, and spectral energy distributions.

For instance, at $B_{AB} \sim 23.5$ the galaxies typically have the spectral energy distributions of Irr galaxies and have $M_V \sim -19.0$ at $z \sim 0.4$. This phenomenon could, however, also be related to a biased galaxy formation process.

4.2. Flat-Spectrum Galaxies

A second major topical question concerns the nature of the bluest galaxies, and specifically whether there exists a population that has distinctly different redshifts from the other galaxies, which might therefore represent a true “primeval” population. This blue population has been referred to as the “Tyson-blue” population, although we stress again that in our observations the colors of faint galaxies are generally much less extreme, and the fraction of objects in this extremely blue population is very much smaller than in Tyson (1988). We have previously stressed the metal-producing capabilities of this population and prefer to refer to it as the population of “flat-spectrum” galaxies (Cowie et al. 1988).

The most extreme examples of flat-spectrum galaxies have SEDs that cannot be fitted by “normal” galaxies, including very blue ones such as NGC 4449, at any redshift $z < 1$. The two objects with $B_{AB} < 24.1$ for which we have failed to obtain a redshift, SSA 22-16 and SSA 22-24, are both in this category. SSA 13-21, which we have not examined spectroscopically, can also not be fitted, and fainter than $B_{AB} \sim 24.1$ there are several further examples. At the faintest levels, however, the photometric uncertainties become large enough that essentially all objects, including many that are nominally as blue as SSA 22-16 and SSA 22-24, can be fitted with a normal galaxy SED.

Within our data set, the “unclassifiable” objects represent only a small fraction (of order 15%) of galaxies at $B_{AB} \leq 24.1$. Regardless of their nature, they cannot therefore contribute significantly to the apparent excess of galaxies at $B \sim 24$, which, as discussed above, has a different explanation involving galaxies at modest redshifts, $z \sim 0.4$.

Because of the continuous distribution of colors seen in the data, these extreme objects lie at the fringes of the general population, leading to considerable difficulty in isolating them as a population. Correspondingly, it is to be expected that any arbitrarily defined set of these blue objects is likely to contain a number of relatively “normal” blue galaxies at modest redshifts. In a previous paper, Cowie et al. (1988) defined a flat-spectrum population in the 22 hr field based on $(B-I)$ color containing SSA 22-10, SSA 22-16, and SSA 22-24, and pointed out that relatively model-independent arguments (Lilly & Cowie 1987) led to the conclusion that objects such as these were responsible for the production of a significant fraction of the metals observed in present-day galaxies. Taking the 18 objects with $(B-I)_{AB} < 0.5$ and $I_{AB} < 25.5$ in the present sample and using the most recent estimates of the light production associated with metal production (Songaila et al. 1990), an average metal production of $0.22 \times 10^{-34} \text{ g cm}^{-3}$, or $\sim 10\%$ of the metals currently seen in spheroids or disks, is indicated. Choice of $(B-I)$ color as the defining characteristic is useful because the significant Balmer break seen between 3700 and 4000 Å in even very blue galaxies means that normal galaxies should only be very blue in $(B-I)$ at very low redshift, $z < 0.2$, or very high redshift, $z > 1.2$, and should be significantly redder at intermediate redshifts because the Balmer break will lie between the B and I passbands.

We now have spectra of the three objects identified by Cowie et al. (1988). SSA 22-10 (Fig. 5) is a low-redshift, low-luminosity extragalactic H II region (see, e.g., Zwicky 1966; Sargent & Searle 1970; Campbell, Terlevich, and Melnick 1986 and references therein). It has extremely strong emission lines, with a rest-frame equivalent width in $[\text{O III}] \lambda 5007$ of 210 Å, and strong lines of $[\text{O II}] \lambda 3727$, $[\text{Ne III}] \lambda 3869$, $\text{H}\gamma \lambda 4340$, $\text{H}\beta \lambda 4861$, $[\text{O III}] \lambda 4959$, $\text{He II} \lambda 5876$, and $\text{H}\alpha \lambda 6563$ are also seen. Once the emission lines are removed, the continuum is well matched by an SED similar to that of NGC 4449. This is shown in Figure 18a, where infrared photometry from Cowie et al. (1990) has been added to the broad-band SED. SSA 22-10 has $M_B \sim -16.3$.

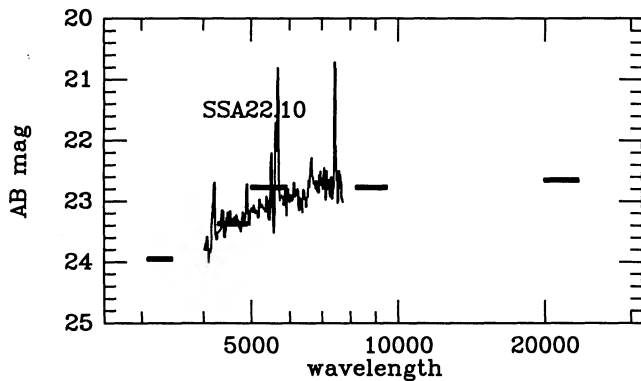


FIG. 18a

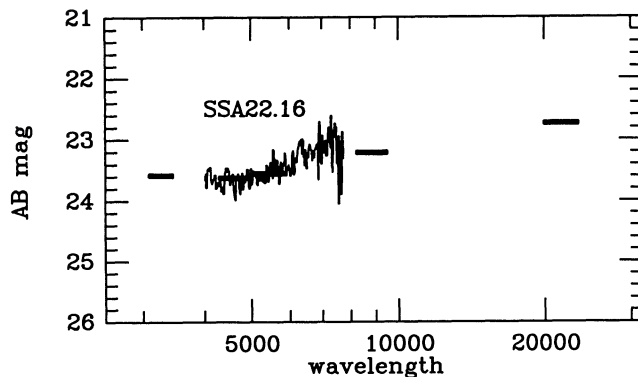


FIG. 18b

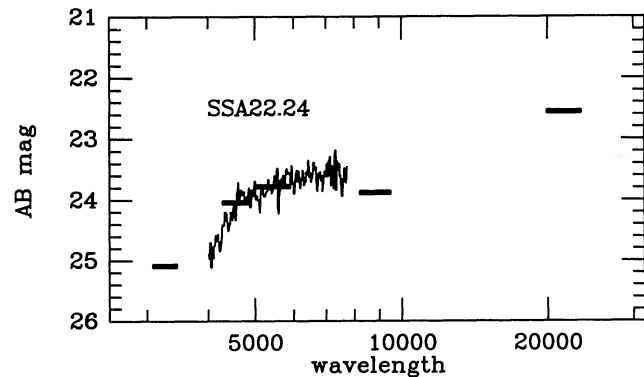


FIG. 18c

FIG. 18.—The Broad-band spectral energy distributions of (a) SSA 22-10, (b) SSA 22-16, and (c) SSA 22-24 from 3400 Å to 2.2 μm. The spectroscopic data have been superposed after the application of an arbitrary scaling in flux density.

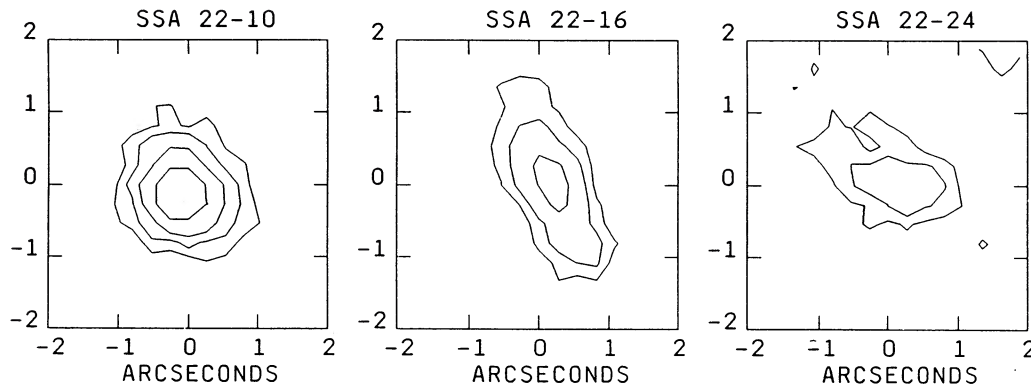


Fig. 19.— V -band morphologies of the photometrically unclassifiable objects in the SSA 22 field. *Left*: SSA 22-10; *middle*: SSA 22-16; *right*: SSA 22-24. Spectroscopically, SSA 22-10 is an extragalactic H II region at $z = 0.13$, while neither SSA 22-16 nor SSA 22-24 can be identified.

In marked contrast, SSA 22-16 and SSA 22-24 have no detectable emission lines (Fig. 5) in the range $4000 \text{ \AA} < \lambda < 8000 \text{ \AA}$ to an observed equivalent width limit of approximately 20 \AA . As mentioned earlier, the emission line in SSA 22-24 reported by Cowie & Lilly (1989) is now known to have been spurious. These two objects also differ markedly from SSA 22-10 in their morphologies (see Fig. 19). SSA 22-10 is compact, with a FWHM of $0''.82$ in their morphologies (see Fig. 19). SSA 22-10 is compact, with a FWHM of $0''.82$ on our best seeing images (which have stellar FWHM of 0.68), and the intrinsic FWHM of this object is probably around $0''.5$, or about 1.5 kpc at $z = 0.13$. This is consistent with the appearance of nearby extragalactic H II regions. In marked contrast, both SSA 22-16 and SSA 22-24 are clearly extended and also noticeably elongated. Both of these objects have intrinsic axial ratios of about $2.5:1$, and both galaxies are barely resolved along their minor axes while having a FWHM along their major axes of $1''.5$ – $2''.0$. There is little doubt that these objects are quite different from SSA 22-10.

The SEDs of SSA 22-16 and SSA 22-24 are also shown in Figures 18*b* and 18*c*. The SED of SSA 22-16 is remarkably flat over almost a decade of wavelength, while that of SSA 22-24 shows both the rollover at shorter wavelengths noted by Cowie & Lilly (1989) and also evidence for a distinct rise into the infrared. Both of these individual SEDs, and the absence of strong emission lines in both objects, are suggestive of high redshifts but are by no means conclusive. In the case of SSA 22-24, the significant spectral break between 4000 and 5000 \AA could be a very strong Balmer break at very low redshift, $z < 0.1$, but the absence at longer wavelengths of a pattern of strong Balmer absorption lines implied by such a strong break makes this option unattractive. There do appear to be two weak absorption features clear of night-sky features at 6011 and 6717 \AA in the spectrum of SSA 22-24. These could be $H\beta$ and $H\gamma$ at $z = 0.383$, and this redshift is superficially attractive because two other galaxies in the 22^h field have this redshift. It would place the Balmer break, which should be strong if the Balmer $H\beta$ and $H\gamma$ lines are strong, longward of 5050 \AA , where no such feature is seen, and would leave completely unexplained the observed break at 4500 \AA . Neither of these low-redshift possibilities can account for the rise in the SED to $2.2 \mu\text{m}$. In fact, the overall SED of SSA 22-24 is rather reminiscent of that of the $z = 3.4$ radio galaxy 0902+34 (Lilly 1988, 1990). Assigning a redshift of about $z \sim 2.7$ to SSA 22-24 would allow the drop in flux shortward of 4500 \AA to be caused by the

Lyman- α forest (see, e.g., Oke & Korycansky 1982), would still have the Lyman limit shortward of the U' passband, and would place the Balmer break and/or 4000 \AA feature at around $1.3 \mu\text{m}$. But a redshift in this range would require a very weak Lyman- α emission line ($EW_0 \leq 6 \text{ \AA}$). The possible absorption lines at 6011 and 6717 \AA do not match the expected ultraviolet absorption features at high z . The Lyman limit at 912 \AA will have passed through the U' band for $z > 2.9$, and while the intrinsic Lyman break can easily be small enough to account for the observed U' flux density, the effects of intervening extrinsic absorption become progressively more serious at higher redshifts. The chance of a galaxy avoiding a strong Lyman-limit system is only about 50% by $z \sim 3.5$ (Sargent, Steidel, and Boksenberg 1989), and SSA 22-24 is very unlikely to have a redshift much higher than this.

In the case of SSA 22-16, there is a suggestion of a weak (0.3 mag) break in the continuum at around 6300 \AA , which could conceivably be a very weak Balmer feature at a redshift of around 0.6 . There is no evidence for an emission-line system at this redshift, however. SSA 22-16 is unlikely to have $z \gg 2$, since the flux stays high all the way through to U' at 3400 \AA .

In summary, we have been unable to determine the redshifts of either SSA 22-16 or SSA 22-24, despite the long spectroscopic integrations obtained on them. The only firm constraints that can be placed on their redshifts come from the requirement that the extrinsic Lyman absorption at high redshifts be consistent with the $(U' - B)$ colors. As noted above, this requires SSA 22-24 to have $z < 3.5$ and SSA 22-16 to have $z < 2$.

Figure 20 shows the $(U' - B)_{AB}/(B - I)_{AB}$ color-color diagram for all the "flat-spectrum" galaxies with $(B - I)_{AB} < 0.67$ and $I_{AB} < 25.5$, highlighting those in the complete $I_{AB} < 24.5$ sample with larger symbols. Galaxies that cannot be photometrically classified as normal galaxies at any $z < 1.25$ are represented as open symbols (including SSA 22-10, which is known to have $z = 0.13$ but whose photometry is contaminated by strong emission lines).

Several points are evident on this diagram. First, there is little overall correlation of $(U' - B)_{AB}$ color with $(B - I)_{AB}$ color. Second, there are very few objects that have a more positive spectral index in $(U' - B)$ than they do in $(B - I)$. Objects generally lie to the left of the locus of power-law spectral energy distributions in the diagram, indicating a steepening of the spectrum shortward of the B band. The best examples of these are SSA 22-24 and SSA 13-21 discussed above, and the slightly

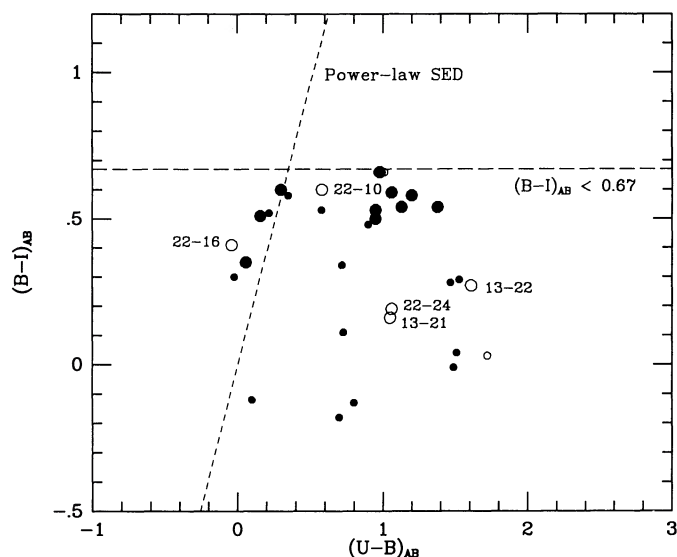


FIG. 20.— $(U-B)_{AB}/(B-I)_{AB}$ two-color diagram for galaxies with $I_{AB} < 25.5$ and $(B-I)_{AB} < 0.67$. Inclined dashed line represents power-law spectral energy distributions. Open symbols represent galaxies that cannot be photometrically classified as normal galaxies at $z < 1.25$. Large symbols represent galaxies with $I_{AB} < 24.5$.

fainter SSA 13-22. Fainter than $I_{AB} \sim 24.5$ (the smaller symbols) there are several more “breaking” galaxies of this type). Third, there are essentially no objects which disappear in the U' band. Finally, objects with $(B-I)_{AB} > 0.5$ can generally be represented by normal galaxy spectral energy distributions. It can be seen that essentially all the objects are thus subject to the same overall redshift constraints as SSA 22-16 and SSA 22-24.

It should, however, be stressed that the $(B-I)$ selection criteria for the “flat-spectrum” population would in any case be biased against galaxies with $z > 3$ because the drop across Lyman- α caused by the Lyman- α forest would be large enough to redden the $(B-I)$ colors, regardless of the effect of the Lyman limit on the $(U-B)$ color. Galaxies at $z > 3$ could well be present in the deep counts but would no longer be expected to be picked out by the flat-spectrum $(B-I)$ condition. For instance, the radio galaxy 0902 + 34 at $z = 3.4$, which is probably undergoing a major star formation episode, has $(B-I)_{AB} \sim 1.5$ (see Lilly 1990).

4.3. The Faintest Galaxies at 26th Magnitude

The nature of the galaxies seen at the faintest levels in deep CCD images is also of paramount interest. Unfortunately, these faintest objects do not have sufficiently accurate photometry for a reliable photometric classification and are beyond the reach of systematic spectroscopic study with the present generation of telescopes. We have already commented that, on the basis of their spectral energy distributions, the majority of these objects could be relatively normal galaxies over a wide range of redshifts. Consequently, only indirect arguments can be made concerning the nature of these objects.

One of the most interesting aspects of these very faint galaxies is their high overall number density. To $B_{AB} \sim 26.5$, there are 2.5×10^5 galaxies deg^{-2} (Fig. 8). This is a conservative estimate of the total surface density of galaxies, since the counts are unlikely to drop to zero, and even if they stopped

rising and stayed at a constant level for a few magnitudes, the total number of galaxies would be substantially increased.

There may already be evidence from the deepest slit profiles obtained in the spectroscopic program for number densities as high as 10^6 deg^{-2} (Cowie & Lilly 1990). At a surface density of $2.5 \times 10^5 \text{ deg}^{-2}$ the average projected object separation is $8''$ (or 80 kpc at cosmological distances), and, as discussed above, there is negligible confusion with good seeing data, and we may thus be reasonably confident that the objects are individual galaxies rather than multiple components of a single entity. This becomes less true as the average image separation ($4''$ at a surface density of 10^6 deg^{-2}) approaches the typical sizes of large galaxies.

As discussed in the previous section, objects seen at B are unlikely to lie at redshifts significantly beyond $z \sim 3$, since the intervening neutral hydrogen absorption rapidly dims objects shortward of Lyman- α for objects at higher redshifts (see, e.g., the radio galaxy 0902 + 34 of Lilly 1989 and the quasars of Oke & Korycansky 1982). The available volume out to $z = 3$ is $7.9 \times 10^7 \text{ Mpc}^3$ for $q_0 = 0.0$ and $2.1 \times 10^7 \text{ Mpc}^3$ for $q_0 = 0.5$, corresponding to average densities of 0.003 and 0.012 Mpc^{-3} , respectively. This is illustrated in Figure 21, where the average comoving density required to accommodate the surface density of galaxies with $B_{AB} < 26.5$ has been computed as a function of the limiting redshift, z_{max} , of the available volume.

The comoving densities required at $B_{AB} < 24.2$ and at $B_{AB} < 2.15$ are also plotted. For these two latter cases, the median redshift is known to be about 0.4 (this work; see above) and 0.2 (Broadhurst et al. 1988), respectively, so the limiting volume containing half the galaxies is actually known. These low-redshift points have been represented as short arcs to account for the remaining uncertainty in the median redshift. On the right-hand axis of this diagram, we have indicated the galaxy luminosity down to which a standard Schechter luminosity function must be integrated in order to achieve the number density indicated on the left-hand axis, taking $\phi^* = 0.0023 \text{ Mpc}^{-3}$.

Koo (1989, 1990) has argued, on the basis of a less deep estimate of the number counts, that the high density of objects required in a flat q_0 geometry argues in favor of an open universe. However, it can be seen in Figure 21 that the high densities indicated at high redshifts are also seen at the much lower redshifts sampled by the spectroscopic surveys, where the choice between $q_0 = 0$ and $q_0 = 0.5$ has only a small effect. Equivalently, the large number of faint galaxies seen at $B_{AB} \sim 26.5$ can be produced if the high densities that are apparently seen at $z \sim 0.4$ are maintained out to $z \sim 1.5$. Nevertheless, within a conventional evolutionary framework, Koo's analyses have highlighted the difficulties of attaining the high surface densities observed.

Clearly the high overall number density of galaxies at $B_{AB} < 26.5$ may be related to the high number density of z systems at $B_{AB} \sim 24$. Regardless of whether the bursting scenario of Broadhurst et al. (1988), introduced to account for the 30% excess at $z \sim 0.2$, can account for the two- to threefold excess at $z = 0.4$, it must run into serious difficulties when applied over the whole cosmological time scale that is likely to be sampled by the $B_{AB} < 26.5$ sample. This is because an object that is visible throughout this period (as is required to produce the high surface density observed) must have sustained high star formation rates (of order $10 M_{\odot} \text{ yr}^{-1}$ at high redshift for a normal initial mass function [IMF] and $B_{AB} < 26.5$) for a cosmological time scale, and is hence unlikely to end up as a

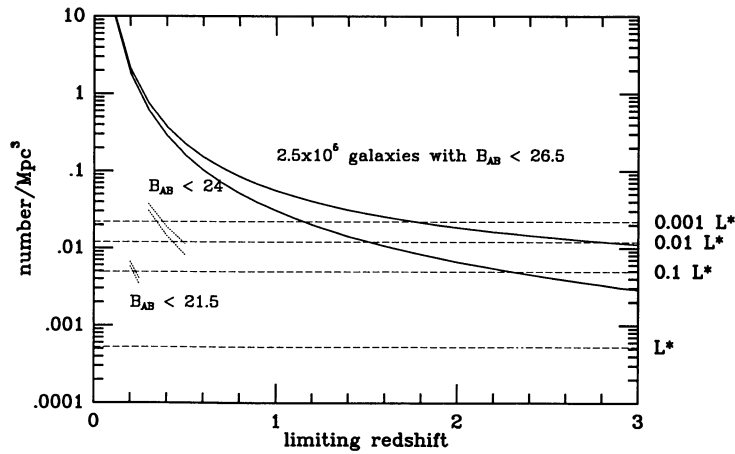


FIG. 21.—Diagram showing the average density required to accommodate the observed high surface density of galaxies at $B < 21.5$, $B > 24$, and $B < 26.5$ as a function of the limiting redshift of the available volume, for $q_0 = 0$ (lower curves) and $q_0 = 0.5$ (upper curves). For galaxies at $B < 21.5$ and $B < 24$, the limiting volumes for half the observed galaxies in these brighter samples are known from their median redshift (from Broadhurst et al. 1988 and the present work), and these are shown as small line segments, reflecting the uncertainty in the median z of the populations. For the $B < 26.5$ galaxies, the redshift distribution is relatively unconstrained, and for these galaxies the required density is shown as a continuous function of the limiting redshift. On the right-hand axis, the luminosity down to which one must integrate the luminosity function to obtain these densities is shown (for $\phi^* \sim 2.3 \times 10^{-3} \text{ Mpc}^{-3}$).

present-day $0.01L^*$ galaxy, unless the IMF is heavily weighted to high-mass stars and the galaxy is particularly efficient at removing the metals produced by the more massive stars. This fundamental difficulty can be seen quantitatively in a relatively model-independent way as follows.

From the monochromatic luminosity of a flat-spectrum galaxy, the overall star formation rate (Cowie 1988) and the return of heavy metals to the interstellar medium (Songaila et al. 1990) can be calculated. Folding in the cosmological time-redshift and magnitude-redshift relations, we can therefore compute, as a function of q_0 , the *minimum* total mass of stars, and the *minimum* total return of metals from a flat-spectrum galaxy that is just visible (above a given magnitude limit) over the redshift range from $z = 0$ to some maximum redshift z_{max} . Recall that our discussion of the comoving densities of objects required to match the high overall surface density of galaxies assumed that the galaxies involved were visible over the whole redshift range $0 < z < z_{\text{max}}$.

The results of this analysis are shown in Figure 22. If $B_{\text{AB}} \sim 26.5$ objects are required to be visible out to $z_{\text{max}} \gg 1$, then high-mass galaxies ($10^{10} M_{\odot}$) with high metal content ($10^8 M_{\odot}$ of metals) will be the result. Notice that while the mass of stars produced (upper pair of curves) will be sensitive to the assumed initial mass function (a Salpeter IMF was used), since the luminosity is produced by high-mass stars whereas the mass is generally accumulated in the lowest mass stars, the production of metals (lower curves) will not be (see, e.g., Songaila et al. 1990), since in this case the luminosity is produced by the same stars that are responsible for the return of metals to the interstellar medium. Hence a $B_{\text{AB}} \sim 26.5$ galaxy visible to high redshifts can only evolve into a present-day dwarf galaxy if it both has a nonstandard initial mass function and is efficient at disposing of its enriched interstellar medium. Note, however, that at very low redshifts this analysis will overestimate the star formation rate because a considerable fraction of the B -band light will come from old and evolved low-mass stars. By $z > 0.5$, however, the assumption that the B -band light in the detected objects is dominated by young stars becomes increasingly correct.

Figures 21 and 22 may now be combined into Figure 23 as follows. We have computed the mass of galaxy down to which a Schechter luminosity function (with $\phi^* = 0.0023 \text{ Mpc}^{-3}$) must be integrated in order for the comoving volume density to satisfy the projected surface densities of galaxies seen at $B_{\text{AB}} < 26.5$, $B_{\text{AB}} < 24$, and $B_{\text{AB}} < 21.5$, using the observed median redshifts to define the available volumes for the last two (as was already done on the right-hand axis of Fig. 21). With the assumption of conservation of the numbers of galaxies, this therefore represents the minimum depth in the luminosity function (i.e., the maximum luminosity of the faintest galaxies) that must be represented by the high-redshift objects as a function of the limiting redshift z_{max} to which the objects are seen. Overlaying the “minimum produced mass” curves from Figure 22 then shows that the requirement of

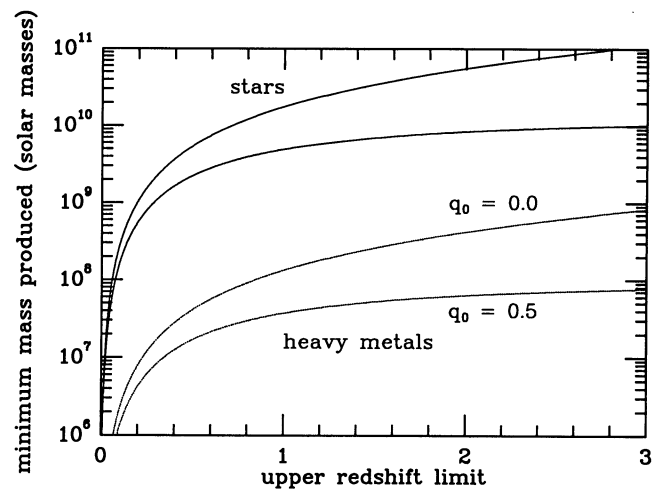


FIG. 22.—Production of stars and metals by a flat-spectrum galaxy that has $B_{\text{AB}} \sim 26.5$ over the whole redshift range out to z_{max} , as a function of z_{max} , for two values of q_0 . The production of stars is sensitive to the assumed initial mass function, but the production of metals is not, since the most massive stars are responsible for both most of the light and also most of the metals.

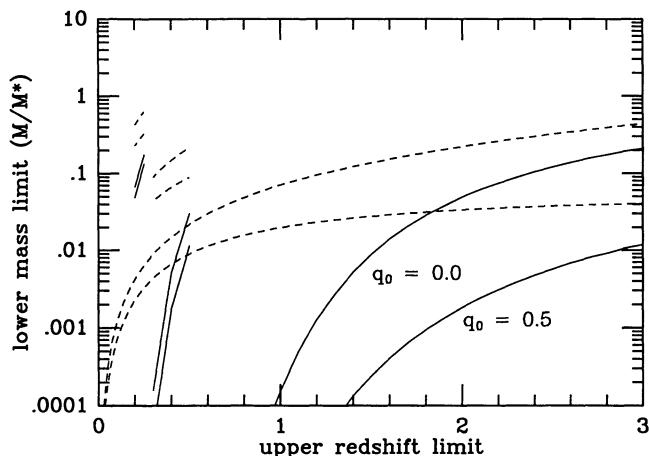


FIG. 23.—Apparent conflict between the high surface density of faint galaxies observed (requiring low-mass galaxy systems) and the high production of mass in systems visible over the visible range. The solid curves represent the minimum depth down the luminosity function that is required (from a Schechter luminosity function with $\phi^* = 0.0023 \text{ Mpc}^{-3}$) to attain the required number densities of galaxies for the three magnitude ranges $B < 21.5$, $B < 24$, and $B < 26.5$ (from Fig. 21). The dashed curves represent the minimum mass produced by flat-spectrum galaxies that are visible above the appropriate magnitude thresholds over the entire volume (from Fig. 22). As in Fig. 21, the $B < 21.5$ and $B < 24$ samples are represented by short arcs reflecting our knowledge of the median redshifts, whereas the $B < 26.5$ sample is represented as a continuous curve. This analysis suggests that, at least in conventional cosmologies, substantial violation of number conservation of galaxies must have occurred, although this is unattractive for the $B < 24$ sample (which is at low redshift).

visibility over the whole redshift range implies that the distant galaxies must evolve into objects that are all significantly more massive than this limit, representing the overproduction of stars and metals alluded to earlier. This suggests that no self-consistent evolutionary model that preserves number density can account for the observed high number density of galaxies seen in faint galaxy samples.

It should be noted that the apparent discrepancy is present even at $B_{AB} \sim 21.5$ where Broadhurst et al. (1988) have successfully fitted such an evolutionary model to their data! This is almost certainly due to the effect of older stellar populations increasing the B -band luminosities of galaxies at low redshift, thus producing an overestimate of the star formation rate in our analysis and hence an overestimate of the masses of the product galaxies. This explanation is more difficult to sustain at $z \sim 0.5$, and is untenable at $z > 1$, where the observed B -band light will be produced only by young stars.

The purpose of this analysis is to show in as model-independent a way as possible that the difficulty of accounting for the high number density of objects, to which others have alluded (see, e.g., Koo 1990), is fundamental and is not simply a product of the choice of parameters in the often complex evolutionary models used by these authors.

The solution may well lie in the widespread merging of smaller units into larger ones. This overcomes this problem because the required density quickly drops to the present density of fairly luminous galaxies.

4.4. Overview: Implications for Galaxy Formation and Evolution

In assessing the impact of these results on our ideas of the formation and evolution of galaxies a distinction should be

drawn between the galaxies seen to $B_{AB} \sim 24$, and those roughly a factor of 10 fainter, which are seen at the limits of deep CCD images at $B_{AB} \sim 26$.

The available evidence in this paper suggests that the excess counts to $B \sim 24$ are a phenomenon associated with moderate-luminosity galaxies at modest redshifts, $z \sim 0.4$, occurring in much larger numbers than expected from the local galaxy population. We stress, however, that the low median redshift at $B_{AB} \sim 24$ that is suggested by our spectroscopic and photometric data needs to be confirmed and better defined with larger samples of objects.

If wholesale merging over the last 5 Gyr is discounted, then the excess objects are not playing a significant role in the formation or evolution of massive (L^*) galaxies. They are simply of too low luminosity and have too high a number density. Indeed, the relative paucity of $0.5 < z < 1.0$ galaxies in the blue-selected samples suggests that there has been only modest evolution in luminous (above L^*) galaxies since the epochs corresponding to $z \sim 1$. This suggests that these galaxies are already well formed and in general relatively stable at $z \sim 1$. This is in accord with recent arguments concerning radio galaxies at $z > 1$ (see, e.g., Lilly 1988, 1990) and is also consistent with the distribution of optical-infrared colors in Cowie et al.'s (1990) K -band-selected sample, which suggests the existence of luminous "old" galaxies at $z \sim 2$.

The physical cause of the excess is still unclear. Widespread bursts of star formation in low-mass galaxies, as suggested by Broadhurst et al. (1988) to account for galaxies at $B_{AB} \sim 21.5$, is a possibility and is supported by the observed distribution of colors. Nevertheless, there are difficulties in adopting this scenario at our fainter levels because of the greater excess of galaxies over nonevolving galaxy populations at $B_{AB} \sim 24$. It may be that some merging is taking place. A nonstandard cosmology also helps, and some galaxies may be the earlier stages of galaxies that do not appear for some reason in local galaxy catalogs. Each of these possibilities has some obvious problems associated with them.

A key question is whether this also holds true at the fainter magnitudes. It should be noted that the majority of these faintest galaxies have colors that are consistent with "normal galaxies" and a large "primeval" high- z population is not necessarily required. Indeed, redshifting out the galaxy population that is seen at $z \sim 0.5$ can largely account for the source counts to $B_{AB} \sim 26.5$. However, the maintenance of the excess density of galaxies over cosmological time scales imposes further constraints, with merging scenarios becoming more attractive than bursts of star formation in low-luminosity galaxies.

The unclassifiable flat-spectrum objects, exemplified by SSA 22-24, remain attractive candidates for a high-redshift population at $z \sim 2$ or greater. Nevertheless, spectroscopic confirmation of this has not yet been possible.

In summary, our strong impression is that a wide range of phenomena are probably present in the faint blue galaxy population including bursts of star formation in dwarf galaxies, the merging of dwarf galaxies into larger units, and the possible presence of very high redshift starburst galaxies. This suggests that attempts to model the population with few-parameter models so as to constrain parameters such as the cosmological geometry or the epoch of galaxy formation are unlikely to succeed.

In fact, the relevance of the faintest galaxies to the origin and evolution of massive galaxies may best be addressed by trying

to identify unambiguously a large population of infrared surveys (see, e.g., Cowie et al. 1990), then, despite the metal production arguments that we have made (e.g., Cowie et al. 1988), this will strongly suggest that the large numbers of blue galaxies at the very faint magnitudes are also not playing a large role in the formation of massive galaxies.

5. SUMMARY

Deep images in four optical passbands (U' , B , V , and I) with limiting magnitudes for galactic images of roughly 27th AB magnitudes have been used to study the population of faint galaxies. Additional spectroscopic data have been obtained for a small subset of objects with $B_{AB} < 24.1$. The chief results can be summarized as follows.

1. While confirming the existence of a blueward trend of galaxy colors at faint magnitudes, $B > 24$, we find that the colors of the faintest galaxies are generally not as blue as found by Tyson (1988). At the faint end the discrepancy is large, almost a magnitude in $(B-I)$. Correspondingly, the fraction of galaxies that cannot be represented as "normal" galaxies is much smaller in our data than in Tyson's.

2. The slope of the B -band source counts appears to decrease below the bright-end slope of 0.465 for magnitudes fainter than $B \sim 24$, thus removing the potential divergence of the integrated night-sky brightness (cf. Tyson 1988).

3. Spectroscopy of a small but representative sample of galaxies with $B_{AB} < 24.1$ (most of which have $B > 23$) has yielded a high success rate for spectroscopic identification and redshift determination. These suggest that the median redshift for this sample is close to 0.4. This is supported by an analysis of the $U' B V I$ spectral energy distributions of a larger sample of galaxies. The only galaxies observed spectroscopically for which a redshift could not be secured were also unclassifiable on the basis of their spectral energy distributions. These were all blue "flat-spectrum" galaxies. The fraction of very high redshift galaxies ($z > 1$) at $B_{AB} < 24.1$ is probably not much larger than 20%.

4. Calculation of the expected slope of the galaxy number counts for conventional cosmologies and with unevolving galaxy populations defined by the faint galaxy populations (either at $20.9 < B_{AB} < 22.4$ or at $23.1 < B < 24.1$) confirms that significant evolution must be occurring even between $B_{AB} \sim 21.5$ and $B_{AB} \sim 23.5$. However, the $23.1 < B_{AB} < 24.1$ population *can* account for the slope of the counts at $B_{AB} > 24$,

if the observed slope of the counts drops below 0.46, as is indicated by the present data.

5. Comparison of the "observed" redshift distribution (seen directly in the spectroscopic observations and inferred from the $U' B V I$ spectral energy distributions) with the nonevolving models derived from both local galaxy populations and the faint $23.1 < B_{AB} < 24.1$ sample of Colless et al. (1989b) show that the evolution is best characterized as an increase in ϕ^* rather than in L^* . This extends the results of Broadhurst et al. (1988) and of Colless et al. (1989b) to much fainter levels. A completely convincing explanation of the physical cause of this effect cannot yet be offered.

6. Of the three "flat-spectrum" galaxies identified by Cowie et al. (1988) as being representative of the production of a significant fraction of the observed heavy elements in the universe, one is a $z = 0.13$ blue compact dwarf with the spectrum of an "extragalactic H II region." The other two remain stubbornly unidentified, including SSA 22-24, for which we had earlier proposed a redshift of 3.4 (Cowie & Lilly 1989) that we have been unable subsequently to confirm. We are able to place only general constraints on the redshifts of these objects.

7. The high number density of very faint galaxies (over $2.5 \times 10^5 \text{ deg}^{-2}$) requires a high comoving density of observable galaxies to be sustained over a large fraction of the available volume to $z \sim 3$. However, suggestions that this may be evidence against $\Omega = 1$ cosmologies (e.g., Koo 1989) need to account for the fact that the required density to accommodate half the observed galaxies at $B_{AB} < 24$ within the median redshift of approximately 0.5 is equally high, in a redshift range where the cosmological effects are of course much smaller. There are fundamental difficulties associated with fitting these galaxies into an evolutionary scenario that preserves the number of galaxies. In particular, even the scenarios of the sort introduced by Broadhurst et al. (1990) whereby the luminosity evolution is concentrated in low-luminosity galaxies probably cannot work, because galaxies visible over the whole Hubble time will result in galaxies that are too massive and that produce too many metals.

We are happy to acknowledge many stimulating discussions with our many colleagues in this field, most particularly with Richard Ellis, David Koo, and Richard Kron. This research was supported by NSF grant 87-18275. Implementation of the TI CCD camera at the University of Hawaii is supported by NSF grant AST86-15631.

REFERENCES

- Baron, E., & White, S. D. M. 1987, *ApJ*, 322, 585
 Broadhurst, T. J., Ellis, R. S., Koo, D. C., & Szalay, A. 1990, *Nature*, 343, 726
 Broadhurst, T. J., Ellis, R. S., & Shanks, T. 1988, *MNRAS*, 235, 827
 Bruzual, G. B. A. 1983, *ApJS*, 53, 497
 Campbell, A., Terlevich, R., & Melnick, J. 1986, *MNRAS*, 223, 811
 Coleman, G. D., Wu, C. C., & Weedman, D. W. 1980, *ApJS*, 43, 393
 Colless, M. M., Ellis, R. S., & Taylor, K. 1989a, in *The Epoch of Galaxy Formation*, ed. C. Frenk, R. Ellis, T. Shanks, A. Heavens, & J. Peacock, (Dordrecht: Kluwer), 359
 Colless, M. M., Ellis, R. S., Taylor, K., & Hook, R. N. 1989b, *MNRAS*, 244, 408
 Cowie, L. L., Gardner, J. P., Lilly, S. J., & McLean, I. S. 1990, *ApJ*, 360, L1
 Cowie, L. L., & Lilly, S. J. 1989, *ApJ*, 336, L41
 ———. 1990, in *The Evolution of the Universe of Galaxies*, ed. R. Kron (Dordrecht: Kluwer), 212
 Cowie, L. L., Lilly, S. J., Gardner, J. P., & McLean, I. S. 1988, *ApJ*, 332, L29
 Efstathiou, G., Ellis, R. S., & Peterson, B. 1988, *MNRAS*, 232, 431
 Ellis, R. S. 1983, in *The Origin and Evolution of Galaxies*, ed. B. Jones & J. Jones (Dordrecht: Reidel), 255
 ———. 1990, in *The Evolution of the Universe of Galaxies*, ed. R. Kron (Dordrecht: Kluwer), 248
 Gardner, J. P., et al. 1991, in preparation.
 Gunn, J. E., & Oke, J. B. 1975, *ApJ*, 195, 255
 Johnson, H. L. 1966, *ARAA*, 4, 193
 Kirshner, R. P., Oemler, A., Schechter, P. L., & Smetman, S. A. 1983, *AJ*, 88, 1285
 Koo, D. C. 1986, *ApJ*, 311, 651
 ———. 1989, in *The Epoch of Galaxy Formation*, ed. C. Frenk, R. Ellis, T. Shanks, A. Heavens, & J. Peacock (Dordrecht: Kluwer), 71
 ———. 1990, in *The Evolution of the Universe of Galaxies*, ed. R. Kron (Dordrecht: Kluwer), 268
 Koo, D. C., & Szalay, A. S. 1984, *ApJ*, 282, 390
 Kron, R. G. 1980, *ApJS*, 43, 305
 Landolt, A. U. 1983, *AJ*, 88, 439
 Lilly, S. J. 1988, *ApJ*, 333, 161
 ———. 1989, *ApJ*, 340, 77
 ———. 1990, in *The Evolution of the Universe of Galaxies*, ed. R. Kron (Dordrecht: Kluwer), 344
 Lilly, S. J., & Cowie, L. L., 1987, in *Infrared Astronomy with Arrays*, ed. C. G. Wynn-Williams & E. E. Becklin (Honolulu: Univ. Hawaii), p. 473
 Lilly, S. J., & Longair, M. S. 1984, *MNRAS*, 211, 833
 Oke, J. B. 1972, *ApJS*, 27, 21
 Oke, J. B., & Korycansky, D. G. 1982, *ApJ*, 255, 11

- Ostriker, J. P. 1990, in *The Evolution of the Universe of Galaxies*, ed. R. Kron (Dordrecht: Kluwer), 25
- Peacock, J. A. 1985, *MNRAS*, 217, 60
- Peebles, P. J. E. 1984, *ApJ*, 284, 439
- Sargent, W. L. W., & Searle, L. 1970, *ApJ*, 160, L155
- Sargent, W. L. W., Steidel, C. C. & Boksenberg, A. 1989, *ApJS*, 69, 703
- Songaila, A., Cowie, L. L., & Lilly, S. J. 1990, *ApJ*, 348, 371
- Stone, R. P. S. 1977, *ApJ*, 218, 767
- Tinsley, B. M. 1980, *ApJ*, 241, 41
- Tyson, J. A. 1988, *AJ*, 96, 1
- Yoshii, Y., & Takahara, F. 1988, *ApJ*, 326, 1
- Zwicky, F. 1966, *ApJ*, 143, 192